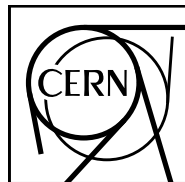


EUROPEAN ORGANISATION FOR NUCLEAR RESEARCH (CERN)



CERN-PH-EP-2014-110

Submitted to: JHEP

Search for strong production of supersymmetric particles in final states with missing transverse momentum and at least three b -jets at $\sqrt{s} = 8$ TeV proton–proton collisions with the ATLAS detector

The ATLAS Collaboration

Abstract

This paper reports the results of a search for strong production of supersymmetric particles in 20.1 fb^{-1} of proton–proton collisions at a centre-of-mass energy of 8 TeV using the ATLAS detector at the LHC. The search is performed separately in events with either zero or at least one high- p_T lepton (electron or muon), large missing transverse momentum, high jet multiplicity and at least three jets identified as originated from the fragmentation of a b -quark. No excess is observed with respect to the Standard Model predictions. The results are interpreted in the context of several supersymmetric models involving gluinos and scalar top and bottom quarks, as well as a mSUGRA/CMSSM model. Gluino masses up to 1340 GeV are excluded, depending on the model, significantly extending the previous ATLAS limits.

Contents

1	Introduction	2
2	SUSY signals	3
3	The ATLAS detector and data sample	6
4	Simulated event samples	6
5	Object reconstruction and identification	8
6	Event selection	9
7	Background estimation	11
7.1	Reducible background	12
7.2	Irreducible background	13
8	Systematic uncertainties	15
9	Results	16
10	Interpretations	26
11	Conclusions	30

1 Introduction

Supersymmetry (SUSY) [1–9] provides an extension of the Standard Model (SM) which can solve the hierarchy problem by introducing supersymmetric partners for the SM bosons and fermions [10–15]. In the framework of the R -parity-conserving minimal supersymmetric extension of the SM (MSSM) [10, 16–19], SUSY particles are produced in pairs and the lightest supersymmetric particle (LSP) is stable. In a large fraction of the MSSM R-parity conserving models, the LSP is the lightest neutralino ($\tilde{\chi}_1^0$)¹ which is weakly interacting, thus providing a possible candidate for dark matter. The coloured superpartners of quarks and gluons, the squarks (\tilde{q}) and gluinos (\tilde{g}), if not too heavy, would be produced in strong interaction processes at the Large Hadron Collider (LHC) and decay via cascades ending with the LSP. The undetected LSP results in missing transverse momentum – whose magnitude is referred to as E_T^{miss} – while the rest of the cascade yields final states with multiple jets and possibly leptons. The scalar partners of the right-handed and left-handed quarks, \tilde{q}_R and \tilde{q}_L , mix to form two mass eigenstates \tilde{q}_1 and \tilde{q}_2 . A substantial mixing is expected between \tilde{t}_R and \tilde{t}_L because of the large Yukawa coupling of the top quark, leading to a large mass splitting between \tilde{t}_1 and \tilde{t}_2 .

SUSY can solve the hierarchy problem by preventing “unnatural” fine-tuning in the Higgs sector provided that the superpartners of the top quark have masses not too far above the weak scale [20, 21]. This condition requires that the gluino is not too heavy in order to limit its contribution to the radiative corrections to the stop masses. Besides, the mass of the left-handed sbottom (\tilde{b}_L) is tied to the stop mass because of the SM weak isospin symmetry. As a consequence, the lightest sbottom (\tilde{b}_1) and stop (\tilde{t}_1) could be produced via strong production with relatively large cross-sections at the LHC, mainly via direct pair production or through $\tilde{g}\tilde{g}$ production followed by $\tilde{g} \rightarrow \tilde{b}_1 b$ or $\tilde{g} \rightarrow \tilde{t}_1 t$ decays.

This paper presents new results of a search for supersymmetry in final states with large E_T^{miss} and at least three jets identified as originated from the fragmentation of a b -quark (b -jets). The previous version of this analysis, using only events with no electrons or muons (0-lepton) in the final state, was performed with the full data set recorded by the ATLAS detector in 2011 at a centre-of-mass energy of 7 TeV [22]. The present analysis uses the dataset of 20.1 fb^{-1} collected during 2012 at a centre-of-mass energy of 8 TeV, and extends the previous search by considering events with at least one high- p_T electron or muon (1-lepton) in the final state.

The results are interpreted in the context of various SUSY models where top or bottom quarks are produced in gluino decay chains. Additional interpretations are provided for a direct sbottom pair production scenario where the sbottom decays into a bottom quark and the next-to-lightest neutralino, $\tilde{\chi}_2^0$, followed by the $\tilde{\chi}_2^0$ decay into a Higgs boson and the LSP, and for a mSUGRA/CMSSM model designed to accommodate a Higgs boson with a mass of about 125 GeV. Exclusion limits in similar SUSY models have been placed by other

¹The SUSY partners of the electroweak gauge and Higgs bosons are called gauginos and higgsinos, respectively. The charged gauginos and higgsinos mix to form charginos ($\tilde{\chi}_i^\pm$, $i = 1, 2$), and the neutral ones mix to form neutralinos ($\tilde{\chi}_j^0$, $j = 1, 2, 3, 4$).

analyses carried out by the ATLAS [23, 24] and CMS [25–28] collaborations with the same integrated luminosity at a centre-of-mass energy of 8 TeV.

2 SUSY signals

In order to confront the experimental measurements with theoretical expectations, several classes of simplified models with b -quarks in the final state are considered. Results from the 0-lepton channel are used to explore all models considered, while the complementarity between the searches in the 0- and 1-lepton channels is used to maximise the sensitivity to models predicting top quarks in the decay chain.

In the first class of simplified models, the lightest stops and sbottoms are lighter than the gluino, such that \tilde{b}_1 and \tilde{t}_1 are produced either in pairs, or via gluino pair production followed by $\tilde{g} \rightarrow \tilde{b}_1 b$ or $\tilde{g} \rightarrow \tilde{t}_1 t$ decays. The mass of the $\tilde{\chi}_1^\pm$ is set at 60 GeV consistently for all models. The following models, also shown in figure 1, are considered:

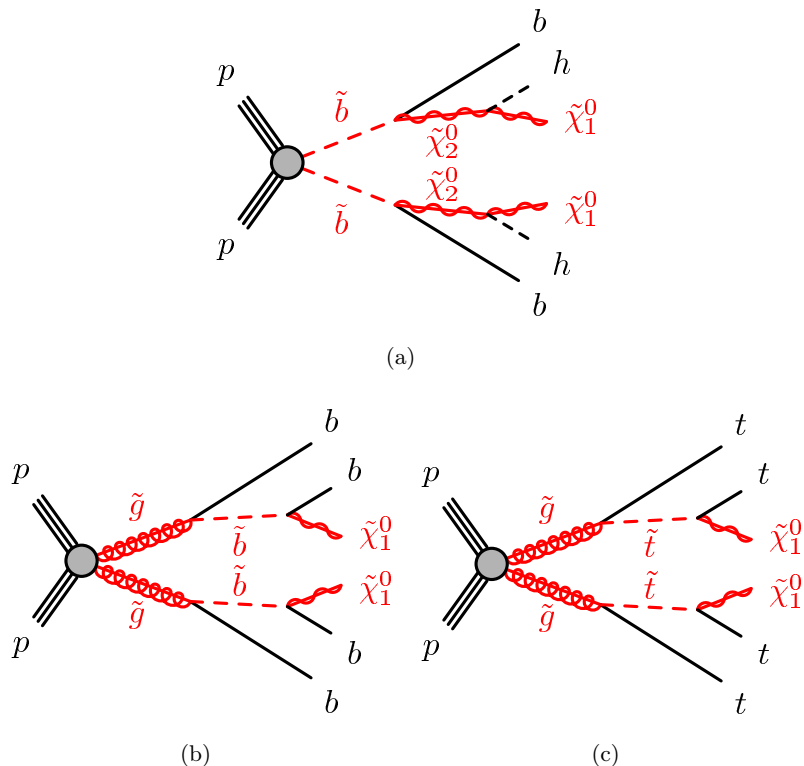


Figure 1. This figure shows the diagrams for the (a) direct-sbottom, (b) gluino-sbottom and (c) gluino-stop scenarios studied in this paper. The different decay modes are discussed in the text.

- **Direct-sbottom model:** in this model, the \tilde{b}_1 is produced in pairs and is assumed to decay exclusively via $\tilde{b}_1 \rightarrow b + \tilde{\chi}_2^0$. The slepton masses are set above a few TeV and only the configuration $m_{\tilde{\chi}_2^0} > m_{\tilde{\chi}_1^0} + m_h$ with a branching ratio for $\tilde{\chi}_2^0 \rightarrow h + \tilde{\chi}_1^0$ of 100% is considered. The mass of the lightest neutral Higgs boson h is set to 125 GeV,

and its decay branching ratios are assumed to be those of the SM Higgs boson. The analysis is mainly sensitive to signal events where both Higgs bosons decay into a $b\bar{b}$ pair, yielding six b -quarks, two neutralinos and no leptons at the end of the decay chain.

- **Gluino–sbottom model:** in this model, the \tilde{b}_1 is the lightest squark, all other squarks are heavier than the gluino, and $m_{\tilde{g}} > m_{\tilde{b}_1} + m_b$ such that the branching ratio for $\tilde{g} \rightarrow \tilde{b}_1 b$ decays is 100%. Sbottoms are produced in pairs or via gluino pair production and are assumed to decay exclusively via $\tilde{b}_1 \rightarrow b\tilde{\chi}_1^0$. The analysis is sensitive to the gluino-mediated production, which has four bottom quarks, two neutralinos and no leptons at the end of the decay chain.
- **Gluino–stop models:** in these models, the \tilde{t}_1 is the lightest squark, all other squarks are heavier than the gluino, and $m_{\tilde{g}} > m_{\tilde{t}_1} + m_t$ such that the branching ratio for $\tilde{g} \rightarrow \tilde{t}_1 t$ decays is 100%. Stops are produced in pairs or via gluino pair production and are assumed to decay exclusively via $\tilde{t}_1 \rightarrow b\tilde{\chi}_1^\pm$ (model I), or via $\tilde{t}_1 \rightarrow t\tilde{\chi}_1^0$ (model II). For the first model, the chargino mass is assumed to be twice the mass of the neutralino, such that the chargino decays into a neutralino and a virtual W boson. The analysis is sensitive to the gluino-mediated production with two top quarks, two bottom quarks, two virtual W bosons and two neutralinos (model I), or four top quarks and two neutralinos (model II) at the end of the SUSY decay chain, yielding signatures with or without leptons.

In the second class of simplified models, all sparticles, apart from the gluino and the neutralino, have masses well above the TeV scale such that the \tilde{t}_1 and the \tilde{b}_1 are only produced off-shell via prompt decay of the gluinos. Thus, the sbottom and stop masses have little impact on the kinematics of the final state. The following models, also shown in figure 2, are considered:

- **Gluino–sbottom off-shell (Gbb) model:** in this model, the \tilde{b}_1 is the lightest squark, but with $m_{\tilde{g}} < m_{\tilde{b}_1}$. A three-body decay $\tilde{g} \rightarrow b\bar{b}\tilde{\chi}_1^0$ via an off-shell sbottom is assumed for the gluino with a branching ratio of 100%. As for the gluino–sbottom model, four bottom quarks, two neutralinos and no leptons are expected at the end of the decay chain. Therefore, only the 0-lepton analysis is used for the interpretation.
- **Gluino–stop off-shell (Gtt) model:** in this model, the \tilde{t}_1 is the lightest squark, but $m_{\tilde{g}} < m_{\tilde{t}_1}$. A three-body decay $\tilde{g} \rightarrow t\bar{t}\tilde{\chi}_1^0$ via an off-shell stop is assumed for the gluino with a branching ratio of 100%. Four top quarks and two neutralinos are expected as decay products of the two gluinos, resulting in signatures with or without leptons.
- **Gluino–stop/sbottom off-shell (Gtb) model:** in this model, the \tilde{b}_1 and \tilde{t}_1 are the lightest squarks, with $m_{\tilde{g}} < m_{\tilde{b}_1, \tilde{t}_1}$. Pair production of gluinos is the only process taken into account, with gluinos decaying via virtual stops or sbottoms, with a branching

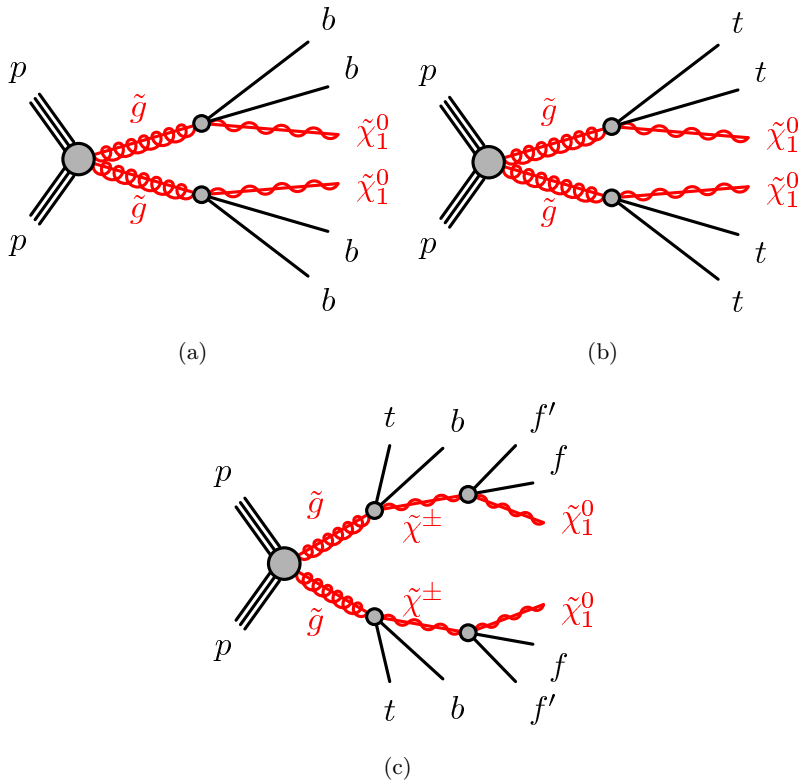


Figure 2. This figure shows the diagrams for the (a) Gbb, (b) Gtt and (c) Gtb scenarios studied in this paper. The different decay modes are discussed in the text.

ratio of 100% assumed for both $\tilde{t}_1 \rightarrow b + \tilde{\chi}_1^\pm$ and $\tilde{b}_1 \rightarrow t + \tilde{\chi}_1^\pm$. The mass difference between charginos and neutralinos is set to 2 GeV, such that the fermions produced in $\tilde{\chi}_1^\pm \rightarrow \tilde{\chi}_1^0 + ff'$ do not contribute to the event selection, and gluino decays result in effectively three-body decays ($bt\tilde{\chi}_1^0$). Two top quarks, two bottom quarks and two neutralinos are expected as decay products of the two gluinos, yielding signatures with or without leptons.

The results are also interpreted in the context of a minimal supergravity model **mSUGRA/CMSSM** [29–34] specified by five parameters: the universal scalar mass m_0 , the universal gaugino mass $m_{1/2}$, the universal trilinear scalar coupling A_0 , the ratio of the vacuum expectation values of the two Higgs fields $\tan\beta$, and the sign of the higgsino mass parameter μ . The model used for interpretation has $A_0 = -2m_0$, $\tan\beta = 30$, $\mu > 0$ and is designed to accommodate a SM Higgs boson with a mass of around 125 GeV, in the $m_0 - m_{1/2}$ range relevant for this analysis.

3 The ATLAS detector and data sample

The ATLAS detector [35] is a multi-purpose particle physics detector with forward-backward symmetric cylindrical geometry.² It consists of inner tracking devices surrounded by a superconducting solenoid, electromagnetic and hadronic calorimeters and a muon spectrometer with a magnetic field produced by three large superconducting toroids each with eight coils. The inner detector, in combination with the 2 T field from the solenoid, provides precision tracking of charged particles for $|\eta| < 2.5$. It consists of a silicon pixel detector, a silicon microstrip detector and a straw-tube tracker that also provides transition radiation measurements for electron identification. The calorimeter system covers the pseudorapidity range $|\eta| < 4.9$. A high-granularity liquid-argon (LAr) sampling calorimeter with lead absorber is used to measure the energy of electromagnetic (EM) showers within $|\eta| < 3.2$. Hadronic showers are measured by an iron/scintillator tile calorimeter in the central region ($|\eta| < 1.7$) and by a LAr calorimeter in the end-cap ($1.5 < |\eta| < 3.2$). The forward region ($3.1 < |\eta| < 4.9$) is instrumented with a LAr calorimeter for both EM and hadronic measurements. The muon spectrometer has separate trigger and high-precision tracking chambers, which provide muon identification and momentum measurement for $|\eta| < 2.7$.

The data sample used in this analysis was recorded during the period from March 2012 to December 2012 with the LHC operating at a pp centre-of-mass energy of 8 TeV. After the application of the data-quality requirements, the total integrated luminosity amounts to 20.1 fb^{-1} , with an associated uncertainty of $\pm 2.8\%$ measured using techniques similar to those detailed in ref. [36], resulting from a preliminary calibration of the luminosity scale using beam-separation scans performed in November 2012. Events for the analysis are selected using a trigger based on a missing transverse momentum selection, which is found to be $> 99\%$ efficient after the offline requirements $E_T^{\text{miss}} > 150 \text{ GeV}$ and at least one reconstructed jet of transverse momentum $p_T > 90 \text{ GeV}$ and $|\eta| < 2.8$.

4 Simulated event samples

Samples of simulated Monte Carlo (MC) events are used to assess the sensitivity to specific SUSY models and aid in the prediction of the SM backgrounds. Jets are labelled as true b -jets in MC simulations if they satisfy the kinematic requirements applied to b -jets detailed in section 5 and if they are matched to a generator-level b -quark with $p_T > 5 \text{ GeV}$ within $\Delta R = 0.3$. The various background processes are then classified into two categories: those leading to final states with at least three true b -jets form the irreducible component while all other processes form the reducible component, the latter being the dominant source of background. Irreducible backgrounds arise mainly from $t\bar{t} + b$ and $t\bar{t} + b\bar{b}$ production, and to a minor extent from $t\bar{t} + Z/h$ followed by $Z/h \rightarrow b\bar{b}$. Their contributions are estimated from MC simulations that are generated inclusively, each event being classified at a later

²ATLAS uses a right-handed coordinate system with its origin at the nominal interaction point (IP) in the centre of the detector and the z -axis along the beam pipe. The x -axis points from the IP to the centre of the LHC ring, and the y -axis points upward. Cylindrical coordinates (r, ϕ) are used in the transverse plane, ϕ being the azimuthal angle around the beam pipe. The pseudorapidity is defined in terms of the polar angle θ as $\eta = -\ln \tan(\theta/2)$, and the distance ΔR in the (η, ϕ) space is defined as $\Delta R = \sqrt{(\Delta\eta)^2 + (\Delta\phi)^2}$.

stage based on the number of true b -jets found. Contributions from background events in which at least one jet is misidentified as a b -jet arise mainly from $t\bar{t}$ production in association with light-parton- and c -jets. Sub-dominant contributions arise from $t\bar{t}$ production in association with $W/Z/h+jets$ (except events with $Z/h \rightarrow b\bar{b}$), single top quark production, $W/Z+jets$ production, and diboson (WW , WZ , ZZ) production. The contributions from all these reducible background processes are estimated simultaneously using a data-driven method described in section 7.1, and MC samples are only used for comparison. Details of the MC simulation samples used in this analysis, as well as the order of cross-section calculations in perturbative QCD (pQCD) used for yield normalisation, are shown in table 1. The background prediction calculated as the sum of the event yield predicted by the MC simulation for each SM process is referred as the MC-only prediction in the following.

Process	Generator + fragmentation/hadronisation	Cross-section order	Tune	PDF set
$t\bar{t}$	POWHEG-r2129 [37–39] + PYTHIA-6.426 [48]	NNLO+NNLL [40–45]	PERUGIA2011C [46]	CT10 [47]
$t\bar{t}^*$	POWHEG-r2129 + HERWIG-6.520 [50]	NNLO+NNLL	AUET2B [49]	CT10
$t\bar{t}^*$	MadGraph-5.1.5.11 [51] + PYTHIA-6.427	NNLO+NNLL	PERUGIA2011C	CT10
Single top				
t -channel	AcerMC-3.8 [52] + PYTHIA-6.426	NNLO+NNLL [53]	AUET2B	CTEQ6L1 [54]
s -channel, Wt	MC@NLO-4.06 [55, 56] + HERWIG-6.520	NNLO+NNLL [57, 58]	AUET2B	CT10
Top+Boson				
$t\bar{t} + W$, $t\bar{t} + Z$	MadGraph-5.1.4.8 + PYTHIA-6.426	NLO [59]	AUET2B	CTEQ6L1
$t\bar{t} + h$	MadGraph-5.1.4.8 + PYTHIA-8.165 [62]	NNLO [60]	AU2 [61]	CTEQ6L1
$W+jets$, $Z+jets$	SHERPA-1.4.1	NNLO [63] with MSTW2008 NNLO [64]	AUET2B	CT10
Dibosons				
WW , WZ , ZZ	SHERPA-1.4.1	NLO [65]	AUET2B	CT10

Table 1. List of MC generators used for the different background processes. Information is given about the pQCD highest-order accuracy used for the normalisation of the different samples, the underlying event tunes and PDF sets considered. Samples labelled with * are employed for the evaluation of systematic uncertainties.

The SUSY signal samples used in this analysis were generated with Herwig++ 2.5.2 [66]. For the Gbb model, in order to ensure an accurate treatment of the initial-state radiation (ISR), MadGraph-5.1.5.4 interfaced to PYTHIA-6.426 is used. All the signal samples were generated with the parton distribution function (PDF) set CTEQ6L1. They are normalised to the signal cross-sections calculated to next-to-leading order in the strong coupling constant, adding the re-summation of soft gluon emission at next-to-leading-logarithmic approximation (NLO+NLL) [67–71].

The nominal cross-section and the uncertainty $\sigma_{\text{theory}}^{\text{SUSY}}$ are taken from an envelope of cross-section predictions using different PDF sets and factorisation and renormalisation scales, as prescribed in ref. [72]. An additional source of systematic uncertainty is taken into account for the Gbb model, where the modelling of the ISR can significantly affect the signal acceptance in the region of the parameter space with small mass splitting Δm between the \tilde{g} and the $\tilde{\chi}_1^0$. The uncertainty on the signal acceptance is estimated by varying the value

of α_S , the renormalisation and factorisation scales, as well as the matching parameters in the MadGraph+PYTHIA-6 MC samples. This uncertainty amounts to 30% for the lowest mass splitting and decreases exponentially with increasing Δm . It is negligible in the region with $\Delta m > 200$ GeV, where the predictions from MadGraph+PYTHIA-6 and Herwig++ are consistent within statistical uncertainties. This systematic uncertainty is negligible for all other signal models considered in this paper.

All the MC samples are processed either through a full simulation of the ATLAS detector [73] based on GEANT4 [74] or a fast simulation [75] that uses a parameterisation of the performance of the ATLAS electromagnetic and hadronic calorimeters and GEANT4 elsewhere. Potential differences between the full and fast simulations were found negligible for this analysis. The effect of multiple p_T interactions in the same or neighbouring bunch crossings (pile-up) is incorporated into the simulation by overlaying additional minimum-bias events generated with PYTHIA-8 onto the hard-scattering process. Simulated events are then weighted to match the observed distribution of the number of p_T interactions, and are reconstructed in exactly the same way as the data otherwise.

5 Object reconstruction and identification

Jets are reconstructed from three-dimensional calorimeter energy clusters with the anti- k_t jet algorithm [76] with a radius parameter $R = 0.4$. The measured jet energy is corrected for inhomogeneities and for the non-compensating response of the calorimeter by differently weighting energy deposits arising from electromagnetic and hadronic showers with correction factors derived from MC simulations and *in situ* measurement in data [77]. Jets are corrected for pile-up using a method proposed in ref. [78]. Finally, additional corrections are applied to calibrate the jet energy to the energy of the corresponding jet of stable particles. Only jets with $|\eta| < 4.5$ and $p_T > 20$ GeV after calibration are retained.

To remove events with jets from detector noise and non-collision backgrounds, events are rejected if they include jets failing to satisfy the loose quality criteria described in ref. [77]. Additional cleaning cuts based on the fraction of the transverse momentum of the jet carried by reconstructed charged particle tracks and the fraction of the jet energy in the EM calorimeter are applied to reject events containing spurious jet signals. Except for the E_T^{miss} computation, only jets with $|\eta| < 2.8$ are further considered.

A neural-network-based algorithm [79] is used to identify jets originated from the fragmentation of a b -quark. It uses as inputs the output weights of different algorithms exploiting the impact parameter of the inner detector tracks, the secondary vertex reconstruction and the topology of b - and c -hadron decays inside the jet. The algorithm used has an efficiency of 70% for tagging b -jets in a MC sample of $t\bar{t}$ events with rejection factors of 137, 5 and 13 against light-quarks, c -quarks and τ leptons respectively. The b -jets are identified within the acceptance of the inner detector ($|\eta| < 2.5$). To compensate for the small differences between the b -tagging efficiencies and the misidentification (mistag) rates in data and MC simulations, correction factors are applied to each jet in the simulations, as described in refs. [79–82]. These corrections are of the order of a few per cent.

Electrons are reconstructed from energy clusters in the electromagnetic calorimeter associated with tracks in the inner detector. Electron candidates are required to have $p_T > 20$ GeV and $|\eta| < 2.47$, and must satisfy the *medium* shower shape and track selection criteria based upon those described in ref. [83], adapted for 2012 data conditions. Muon candidates are identified using a match between an extrapolated inner detector track and one or more track segments in the muon spectrometer [84], and are required to have $p_T > 10$ GeV and $|\eta| < 2.5$. In order to reduce the contributions from semileptonic decays of hadrons, lepton candidates found within $\Delta R = 0.4$ of a jet are discarded. Events containing one or more muon candidates that have a transverse (longitudinal) impact parameter d_0 (z_0) with respect to the primary vertex larger than 0.2 (1) mm are rejected to suppress cosmic rays. *Signal* electrons (muons) are required to be isolated, i.e. the sum of the extra transverse energy deposits in the calorimeter, corrected for pile-up effects, within a cone of $\Delta R = 0.3$ around the lepton candidate must be less than 18% (23%) of the lepton p_T , and the scalar sum of the transverse momenta of tracks within a cone of $\Delta R = 0.3$ around the lepton candidate must be less than 16% (12%) of the lepton p_T . Energy deposits and tracks of the leptons themselves are not included. In addition, to further suppress leptons originating from secondary vertices, signal electrons (muons) must have $|z_0 \sin \theta| < 0.4$ mm and $d_0/\sigma_{d_0} < 5(3)$. Signal electrons must also satisfy tighter quality requirements based upon the criteria denoted by *tight* in ref. [83]. Correction factors are applied to MC events to match the lepton identification and reconstruction efficiencies observed in data.

The measurement of the missing transverse momentum vector (and its magnitude E_T^{miss}) is based on the transverse momenta of all jets, electron and muon candidates, and all calorimeter clusters not associated with such objects. Clusters associated with either electrons or photons with $p_T > 10$ GeV, and those associated with jets with $p_T > 20$ GeV, make use of the calibrations of these respective objects. Clusters not associated with these objects are calibrated using both calorimeter and tracker information [85].

6 Event selection

Following the trigger and object selection requirements described in sections 3 and 5, events are discarded if they fail to satisfy basic quality criteria designed to reject detector noise and non-collision backgrounds. Candidate events are required to have a reconstructed primary vertex associated with five or more tracks with $p_T > 0.4$ GeV [86]; when more than one such vertex is found, the vertex with the largest summed p_T^2 of the associated tracks is chosen as the primary vertex. Events must have $E_T^{\text{miss}} > 150$ GeV and at least four jets with $p_T > 30$ GeV. The leading jet is required to have $p_T > 90$ GeV and at least three of the jets with $p_T > 30$ GeV must be b -tagged. The events selected at this stage are then divided into two complementary channels based on the number of leptons: i) 0-lepton channel, formed by events with no reconstructed electron or muon candidates; and ii) 1-lepton channel, formed by events with at least one signal lepton with $p_T > 25$ GeV. After this basic selection, events are classified into several signal regions (SR), designed to provide sensitivity to the different kinematic topologies associated with the various SUSY models

under study. Each SR is defined by a set of selection criteria using additional event-level variables calculated from the reconstructed objects.

For the 0-lepton channel, four additional variables are used:

- The inclusive effective mass $m_{\text{eff}}^{\text{incl}}$, defined as the scalar sum of the $E_{\text{T}}^{\text{miss}}$ and the p_{T} of all jets with $p_{\text{T}} > 30$ GeV. It is correlated with the overall mass scale of the hard-scatter interaction and provides good discrimination against SM background.
- The exclusive effective mass m_{eff}^{4j} , defined as the scalar sum of the $E_{\text{T}}^{\text{miss}}$ and the p_{T} of the four leading jets. It is used to suppress the multi-jet background and to define the SRs targeting SUSY signals where exactly four b -jets and large $E_{\text{T}}^{\text{miss}}$ are expected in the final state.
- $\Delta\phi_{\text{min}}^{4j}$, defined as the minimum azimuthal separation between any of the four leading jets and the missing transverse momentum direction. To remove multi-jet events where $E_{\text{T}}^{\text{miss}}$ results from poorly reconstructed jets or from neutrinos emitted close to the direction of the jet axis, events are required to have $\Delta\phi_{\text{min}}^{4j} > 0.5$ and $E_{\text{T}}^{\text{miss}}/m_{\text{eff}}^{4j} > 0.2$. The combination of these two requirements reduces the contribution of the multi-jet background to a negligible amount.
- The missing transverse momentum significance, defined as $E_{\text{T}}^{\text{miss}}/\sqrt{H_{\text{T}}^{4j}}$, where H_{T}^{4j} is the scalar sum of the transverse momenta of the four leading jets, is used to define the SRs aiming at SUSY signals with four jets in the final state.

For the 1-lepton channel, event selections are defined using the following variables:

- $m_{\text{eff}}^{\text{incl}}$, defined as for the 0-lepton channel with the addition of the p_{T} of all signal leptons with $p_{\text{T}} > 20$ GeV.
- The transverse mass m_{T} computed from the leading lepton and the missing transverse momentum as $m_{\text{T}} = \sqrt{2p_{\text{T}}^{\ell}E_{\text{T}}^{\text{miss}}(1 - \cos\Delta\phi(\ell, E_{\text{T}}^{\text{miss}}))}$. It is used to reject the main background from $t\bar{t}$ events where one of the W bosons decays leptonically. After the m_{T} requirement, the dominant contribution to the $t\bar{t}$ background in the 1-lepton channel arises from dileptonic $t\bar{t}$ events.

The baseline event selections for each channel and the nine resulting SRs are summarised in table 2. Three sets of SRs, two for the 0-lepton channel and one for the 1-lepton channel, each denoted by ‘0 ℓ ’ or ‘1 ℓ ’, respectively, are defined to enhance the sensitivity to the various models considered. They are characterised by having relatively hard $E_{\text{T}}^{\text{miss}}$ requirements and at least four (SR-0 ℓ -4j), six (SR-1 ℓ -6j) or seven (SR-0 ℓ -7j) jets, amongst which at least three are b -jets. Signal regions with zero leptons and at least four jets target SUSY models with sbottoms in the decay chain, while the 1-lepton and the 0-lepton–7-jets SRs aim to probe SUSY models predicting top quarks in the decay chain. All SRs are further classified as A/B/C depending on the thresholds applied to the various kinematic variables previously defined, designed to target different mass hierarchies in the various

scenarios considered. In particular, a dedicated SR aiming to increase the sensitivity at low mass splitting between the gluino and the $\tilde{\chi}_1^0$ in the Gbb model is defined. This SR (denoted by SR-0 ℓ -4j-C* in table 2) exploits the recoil against an ISR jet by requiring the leading jet to fail the b -tagging requirements.

Baseline 0-lepton selection: lepton veto, $p_T^{j_1} > 90$ GeV, $E_T^{\text{miss}} > 150$ GeV, ≥ 4 jets with $p_T > 30$ GeV, $\Delta\phi_{\min}^{4j} > 0.5$, $E_T^{\text{miss}}/m_{\text{eff}}^{4j} > 0.2$, ≥ 3 b -jets with $p_T > 30$ GeV			
N jets (p_T [GeV])	E_T^{miss} [GeV]	m_{eff} [GeV]	$E_T^{\text{miss}}/\sqrt{H_T^{4j}}$ [$\sqrt{\text{GeV}}$]
SR-0 ℓ -4j-A	≥ 4 (50)	> 250	$m_{\text{eff}}^{4j} > 1300$
SR-0 ℓ -4j-B	≥ 4 (50)	> 350	$m_{\text{eff}}^{4j} > 1100$
SR-0 ℓ -4j-C*	≥ 4 (30)	> 400	$m_{\text{eff}}^{4j} > 1000$
SR-0 ℓ -7j-A	≥ 7 (30)	> 200	$m_{\text{eff}}^{\text{incl}} > 1000$
SR-0 ℓ -7j-B	≥ 7 (30)	> 350	$m_{\text{eff}}^{\text{incl}} > 1000$
SR-0 ℓ -7j-C	≥ 7 (30)	> 250	$m_{\text{eff}}^{\text{incl}} > 1500$
Baseline 1-lepton selection: ≥ 1 signal lepton (e, μ), $p_T^{j_1} > 90$ GeV, $E_T^{\text{miss}} > 150$ GeV, ≥ 4 jets with $p_T > 30$ GeV, ≥ 3 b -jets with $p_T > 30$ GeV			
N jets (p_T [GeV])	E_T^{miss} [GeV]	m_T [GeV]	$m_{\text{eff}}^{\text{incl}}$ [GeV]
SR-1 ℓ -6j-A	≥ 6 (30)	> 175	> 140
SR-1 ℓ -6j-B	≥ 6 (30)	> 225	> 140
SR-1 ℓ -6j-C	≥ 6 (30)	> 275	> 160

Table 2. Definition of the signal regions used in the 0-lepton and 1-lepton selections. The jet p_T threshold requirements are also applied to b -jets. The notation SR-0 ℓ -4j-C* means that the leading jet is required to fail the b -tagging requirements to target the region close to the kinematic boundary in the Gbb model.

7 Background estimation

The main source of reducible background is the production of $t\bar{t}$ events where a c -jet or a hadronically decaying τ lepton is mistagged as a b -jet, the contribution from $t\bar{t}$ events with a light-quark or gluon jet mistagged as a b -jet being relatively small. In the 0-lepton channel, most of these $t\bar{t}$ events have a W boson decaying leptonically where the lepton is not reconstructed, is outside the acceptance, is misidentified as a jet, or is a τ lepton which decays hadronically. In the 1-lepton channel, the high m_T requirement used to define the SRs enhances the contribution from dileptonic $t\bar{t}$ events, where one of the two leptons is a hadronically decaying τ lepton. Additional minor sources of reducible background are single-top production, $t\bar{t}+W/Z/h$ (except events with $Z/h \rightarrow b\bar{b}$), $W/Z+\text{heavy-flavour}$ jets, and diboson events. The irreducible backgrounds with at least three true b -jets in the final state arise predominantly from $t\bar{t}+b/b\bar{b}$ events, and to a minor extent from $t\bar{t}+Z/h$ production with a subsequent decay of the Z or Higgs boson into a pair of b -quarks.

Different techniques are used to estimate the contribution from the reducible and the irreducible backgrounds in the SRs, explained in detail in the following sections.

7.1 Reducible background

All reducible backgrounds are estimated simultaneously using a data-driven method which predicts the contribution from events with at least one mistagged jet amongst the three selected b -jets. This estimate is based on a matrix method (MM) similar to that used in ref. [87] to predict the contribution from background events with fake and non-prompt leptons. It consists of solving a system of equations relating the number of events with N_j jets and N_b b -jets to the number of events with N_b^T true b -jets and $(N_j - N_b^T)$ non-true b -jets, prior to any b -tagging requirement. This method is applied on an event-by-event basis, such that for a given event containing N_j jets satisfying the η and p_T requirements applied to b -jets, 2^{N_j} linear equations are necessary to take into account the possibility for each of the N_j jets to be a true b -jet or not. These linear equations are written in the form of a matrix of dimension $2^{N_j} \times 2^{N_j}$, the elements of which are functions of the probabilities for each jet in the event to be tagged or mistagged as a b -jet. The system of 2^{N_j} equations is solved by inverting the matrix, and an event weight is calculated from the combinations containing zero, one or two true b -jets. The weights obtained for each event satisfying all selection criteria except the b -tagging requirements are then summed to obtain the predicted number of events with at least one mistagged b -jet amongst the selected b -jets.

The b -tagging efficiencies used in the MM are measured in data for each jet-flavour using different techniques [79–81]. They are labelled as ϵ_b , ϵ_c , ϵ_τ and ϵ_l for b -, c -, τ - and light-parton-jets respectively. However, since the origin of a jet candidate is unknown in data, a mistag rate based on MC simulations which takes into account the relative contribution of each source of non-true b -jets is derived. The average mistag rate ϵ_f is defined in terms of the various jet-flavour efficiencies as $\epsilon_f = f_\tau \epsilon_\tau + f_c \epsilon_c + f_l \epsilon_l$, where f_τ , f_c and f_l are the relative fractions of each jet-flavour prior to any b -tagging requirement. Since the reducible background is dominated by $t\bar{t}$ events, the relative jet-flavour fractions are extracted from the $t\bar{t}$ MC sample described in section 4, separately for each lepton multiplicity. In events containing zero or one lepton, they are obtained as a function of the jet p_T and $|\eta|$, and as a function of the jet multiplicity to take into account the dependence with the number of additional partons produced in the hard-scattering or in the radiations. In events with exactly one lepton, the contribution from hadronic τ -jets arising from the second W boson decay increases in events with $m_T > m(W)$ and therefore the relative fractions of each jet-flavour are additionally binned as a function of the transverse mass. Events with two leptons are present in the inclusive 1-lepton SRs and in a 2-lepton control region (CR) used for the determination of the dominant irreducible background contribution. This CR is obtained by requiring $m_T < 140$ GeV to prevent overlap with the 1-lepton SRs as detailed in section 7.2. In dileptonic $t\bar{t}$ events, both W bosons decay into an electron, a muon or a leptonically decaying τ and mistagged b -jets can only come from additional c - or light-parton-jets. Consequently, the jet-flavour fractions are only parameterised as a function of the jet p_T and η in events with two leptons.

Alternatively, the average mistag rates are determined in data using 0, 1 and 2-lepton regions enriched in $t\bar{t}$ events. These regions are defined following the same requirements as for the baseline event selection for all channels, except that events are required to have at least two b -jets and E_T^{miss} between 100 GeV and 200 GeV in order to minimise any possible contribution from signal events in the data. To estimate the mistag rate, the contribution from events with at least three true b -jets is subtracted using MC simulations. The mistag rate is measured as the probability to have a third b -jet in bins of p_T and $|\eta|$, and an additional parameterisation as a function of m_T is used in the 1-lepton channel. The results obtained with this method are consistent with the ones based on MC simulations. Because of the low number of events in data, the mistag rate estimated from MC simulations using the jet-flavour fractions method is taken as baseline, and the difference with the measurement in data is treated as a systematic uncertainty.

This procedure was validated using the inclusive sample of simulated $t\bar{t}$ events described in section 4 as follows. The MM is applied to the entire MC sample to predict the number of events with at least one mistagged b -jet. The contribution from the irreducible $t\bar{t} + b/b\bar{b}$ background is extracted from the same sample as detailed in section 4, and the sum of the two components is compared to the inclusive event yield of the MC sample. Good agreement is found, at preselection level and also at various steps in the event selection chain.

7.2 Irreducible background

The estimate of the minor contribution from $t\bar{t} + Z/h$ production followed by $Z/h \rightarrow b\bar{b}$ relies on MC predictions normalised to their theoretical cross-sections, while the dominant irreducible background from $t\bar{t} + b/b\bar{b}$ events is estimated by normalising the MC predictions to the observed data in a CR. The CR, common to all SRs in both the 0- and 1-lepton channels, is defined using events with exactly two signal leptons and at least four jets with $p_T > 30$ GeV, at least one of them being required to have $p_T > 90$ GeV and three of them to be b -tagged. The E_T^{miss} threshold is relaxed to 100 GeV to increase the sample size, and the transverse mass is required to be less than 140 GeV to remove the overlap with the 1-lepton SRs and to reduce the potential contamination from signal events to below a few per cent. The trigger efficiency is above 90% in the CR and a systematic uncertainty of 2% is added to account for a small difference between the trigger turn-on curves in data and MC simulations in the 100–150 GeV E_T^{miss} range. Figure 3 shows the m_T distribution in the CR, before the requirement of $m_T < 140$ GeV; the jet multiplicity, the E_T^{miss} , and the $m_{\text{eff}}^{\text{incl}}$ distributions with $m_T < 140$ GeV are also shown.

The expected number of $t\bar{t} + b/b\bar{b}$ events in the various SRs is estimated via a profile likelihood fit [88] to the events in the 2-lepton CR. The expected and observed numbers of events in the CR are described by Poisson probability functions. The statistical and systematic uncertainties on the expected values described in section 8 are treated as nuisance parameters and are constrained by a Gaussian function with a width corresponding to the size of the uncertainty considered, taking into account the correlations between these parameters. The likelihood function is built as the product of the Poisson probability functions and the constraints on the nuisance parameters. The free parameter is the overall

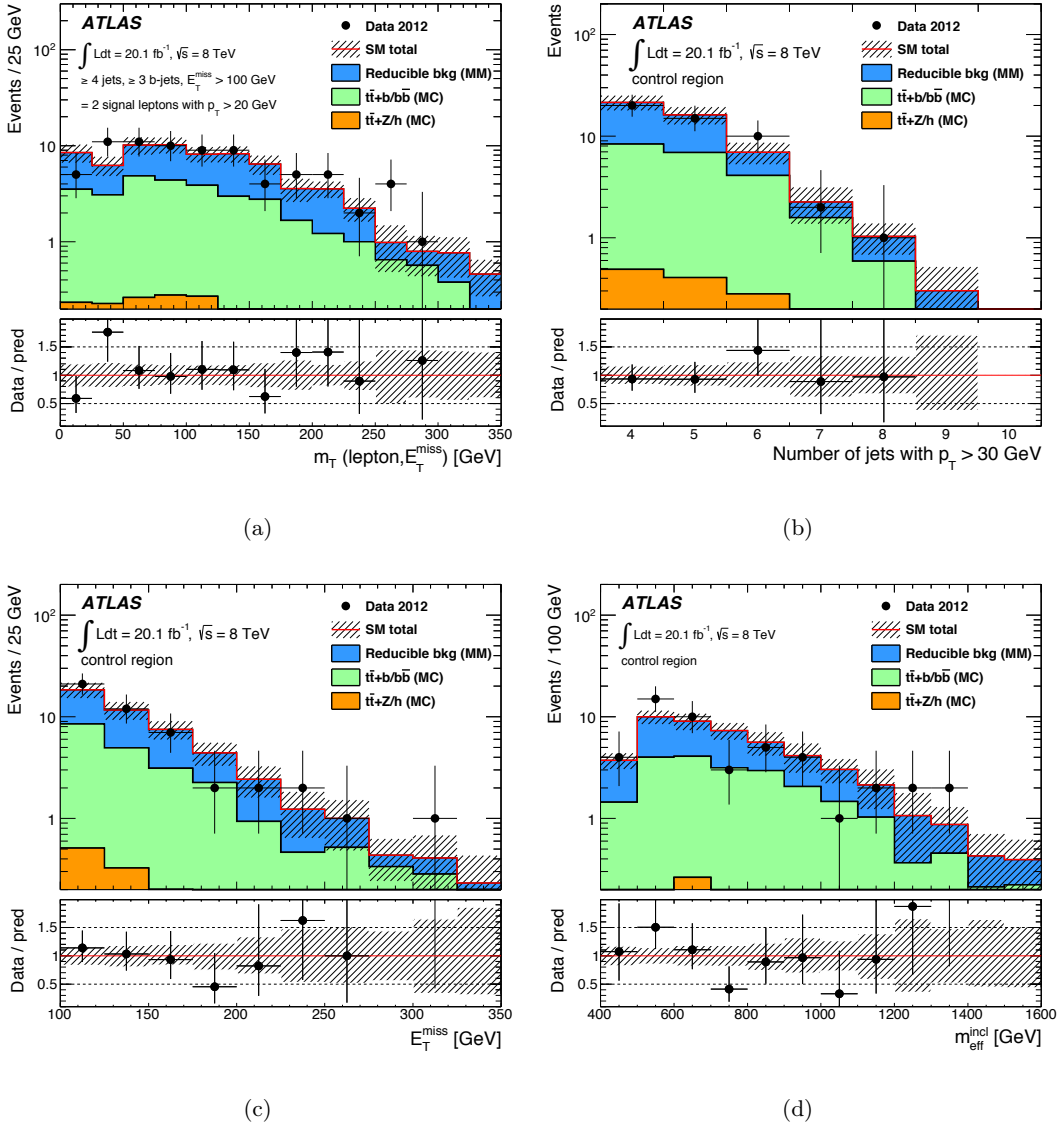


Figure 3. Expected distributions of SM background events and observed data distributions in the 2-lepton control region. The distributions of (a) m_T prior to the requirement on this variable, and (b) the number of jets with $p_T > 30$ GeV, (c) E_T^{miss} and (d) $m_{\text{eff}}^{\text{incl}}$ are shown. Also displayed are the respective contributions of the backgrounds described in the legend and the ratio between the expected and observed event yields. The shaded bands include all experimental systematic uncertainties on the MC and MM predictions. The normalisation of the irreducible background $t\bar{t} + b/b\bar{b}$ is as predicted by its theoretical cross-section scaled to the same luminosity as the data, prior to the fit in the control region.

normalisation of the $t\bar{t} + b/b\bar{b}$ background, while the normalisations of the remaining irreducible and reducible backgrounds are initially set to their predictions and allowed to vary within their systematic uncertainties. The result of the fit in the CR is summarised in

table 3. Given the good agreement between the expected and observed yields, the fit gives a negligible correction to the normalisation of the $t\bar{t} + b/b\bar{b}$ background. The uncertainty on the total background estimate is smaller than the largest individual uncertainty due to anticorrelations between the uncertainties on the reducible and irreducible backgrounds.

	Before the fit	After the fit
Observed events	48	48
Total background events	48	48 ± 7
Reducible background events	27	27 ± 7
$t\bar{t} + b/b\bar{b}$ events	20	20 ± 10
$t\bar{t} + (Z \rightarrow b\bar{b})$ events	0.5	0.5 ± 0.2
$t\bar{t} + (h \rightarrow b\bar{b})$ events	0.9	0.9 ± 0.9
MC-only prediction	50	-

Table 3. Background fit result in the $t\bar{t} + b/b\bar{b}$ CR. Uncertainties quoted include statistical and detector-related systematic effects. The MC-only prediction is given for comparison.

8 Systematic uncertainties

The dominant detector-related systematic uncertainties on the amount of irreducible background are due to the jet energy scale (JES) and resolution (JER) uncertainties; they range respectively from 16% to 37% and from 1% to 32% in the various SRs before the fit. The JES uncertainty is derived from a combination of simulations, test beam data and *in situ* measurements [77, 89]. Additional contributions accounting for the jet-flavour composition, the calorimeter response to different jet-flavours, pile-up and b -jet calibration uncertainties are also taken into account. Uncertainties on the JER are obtained with an *in situ* measurement of the jet response asymmetry in dijet events. Uncertainties in jet measurements are propagated to the E_T^{miss} , and additional subdominant uncertainties on E_T^{miss} arising from energy deposits not associated with any reconstructed objects are also included. The uncertainty associated with b -jets is evaluated by varying the p_T - and flavour-dependent correction factors applied to each jet in the simulation within a range that reflects the systematic uncertainty on the measured tagging efficiencies and mistag rates. It varies between 10% and 16% in the different SRs for the irreducible background, but it largely cancels for the $t\bar{t} + b/b\bar{b}$ background because of the normalisation in the CR. Uncertainties in lepton reconstruction and momentum scales are negligible. All these experimental systematic uncertainties are treated as fully correlated between the signal and the irreducible backgrounds extracted from MC simulations.

Additional theoretical systematic uncertainties are considered for the irreducible backgrounds. The uncertainty on the $t\bar{t} + b/b\bar{b}$ cross-section cancels in the normalisation of the MC simulation in the CR, and only the theoretical uncertainties on the MC prediction used to extrapolate from the CR to the SRs are considered. The uncertainty due to the

choice of the factorisation (μ_F) and renormalisation (μ_R) scales in POWHEG are estimated by comparing the baseline sample to POWHEG+PYTHIA-6 samples generated with μ_F and μ_R varied separately up and down by a factor of two, giving an uncertainty of up to 13%. The uncertainty due to the choice of MC generator is estimated by comparing the estimate from the nominal POWHEG+PYTHIA-6 sample to the MadGraph+PYTHIA-6 sample generated with up to three additional partons at the matrix-element level, yielding an uncertainty of up to 30%. The parton shower uncertainty is assessed by comparing POWHEG interfaced to PYTHIA-6 with POWHEG interfaced to HERWIG and JIMMY, and amounts up to 65% in the SRs where at least seven jets are required. The PDF uncertainties are derived following the Hessian method [90], resulting in an uncertainty of less than 2% for all SRs.

The theoretical uncertainty on the $t\bar{t} + Z$ cross-section is 22% [59]. The systematic uncertainties associated with the modelling of $t\bar{t} + Z$ events are estimated by using different MadGraph+PYTHIA-6 samples: variations up and down of the μ_R and μ_F by a factor of two result in an uncertainty of up to 50%; variations of the ISR/FSR parameters within ranges validated by measurements in data yield an uncertainty of up to 50% for each variation; variations up and down of the matrix-element to parton-shower matching parameter x_{qcut} by 5 GeV around the central value of 20 GeV result in an uncertainty of up to 30%. For the small contribution from the $t\bar{t} + h(\rightarrow b\bar{b})$ background, a total uncertainty of 100% is assumed to account for large uncertainties on the acceptance, while the inclusive cross-section is known to better precision.

Systematic uncertainties on the MM prediction of the reducible backgrounds include the uncertainties on the measurement of the b -tagging efficiency for the different jet-flavours. They vary in the range between 4% and 14% and are treated as fully correlated with the irreducible background and the signal. The statistical uncertainty of the $t\bar{t}$ MC sample used to extract the jet-flavour fractions is also taken into account and is of the order of 1%. The difference between the baseline prediction obtained with the mistag rate from simulated $t\bar{t}$ events and the prediction obtained using the mistag rate measured in data is assigned as a systematic uncertainty. This uncertainty ranges from 9% to 45% in the different SRs. Finally, the statistical uncertainty on the number of observed events for each b -jet multiplicity is propagated to the MM prediction. This latter uncertainty is the dominant source of uncertainty on the background estimation in most SRs.

9 Results

The data are compared to the background predictions in figures 4–10. Figure 4 shows the observed distributions of the number of jets with $p_T > 30$ GeV, m_{eff}^{4j} and E_T^{miss} after the 0-lepton baseline selection detailed in table 2, together with the background prediction from the MM for the reducible background and from MC simulations for the irreducible background. Figure 5 shows the same distributions for events with at least four jets with $p_T > 50$ GeV and three b -jets with $p_T > 50$ GeV after the 0-lepton baseline selection. The $m_{\text{eff}}^{\text{incl}}$ and E_T^{miss} distributions with a requirement of at least seven jets with $p_T > 30$ GeV after the 0-lepton baseline selection are shown in figure 6. Figure 7 shows the number of

jets with $p_T > 30$ GeV after the 1-lepton baseline selection, as well as the distributions of m_T , E_T^{miss} and $m_{\text{eff}}^{\text{incl}}$ after requiring at least six jets with $p_T > 30$ GeV in addition to the 1-lepton baseline selection. The m_{eff}^{4j} , $m_{\text{eff}}^{\text{incl}}$ and E_T^{miss} distributions obtained before the final requirement on these quantities are shown in figures 8–10, representing each SR. Also shown in all figures are the predictions of two benchmark signal models.

The background prediction in each SR is obtained by adding the Poisson probability function describing the expected number of events in the SR and the corresponding nuisance parameters in the likelihood fit. The results of the fits and the observed data in each SR are reported in tables 4 and 5 for the 0-lepton and 1-lepton channels, respectively. No significant deviation from the SM expectation is observed in any of the 0-lepton SRs. In the 1-lepton channel, a deficit in data is observed in all overlapping SRs. In addition to the event yields, the CL_b -values [91], which quantify the observed level of agreement with the expected yield, and the p_0 -values, which represent the probability of the SM background alone to fluctuate to the observed number of events or higher, are also reported. The p_0 -values are truncated at 0.5 if the number of observed events is below the number of expected events. Upper limits at 95% confidence level (CL) on the number of beyond-the-SM (BSM) events are derived in each SR using the CL_s prescription [91] and neglecting any possible signal contamination in the CR. These are obtained with a fit in each SR which proceeds in the same way as the fit used to predict the background, except that the number of events observed in the SR is added as an input to the fit, and an additional parameter for the non-SM signal strength, constrained to be non-negative, is fit. The upper limits are derived with pseudo-experiments, and the results obtained with an asymptotic approximation [88] are given in parentheses for comparison. These limits, after being normalised by the integrated luminosity of the data sample, can be interpreted in terms of upper limits on the visible cross-section for hypothetical BSM contributions, defined in terms of the kinematic acceptance A and the experimental efficiency ϵ as $\sigma_{\text{vis}} = \sigma \times A \times \epsilon$.

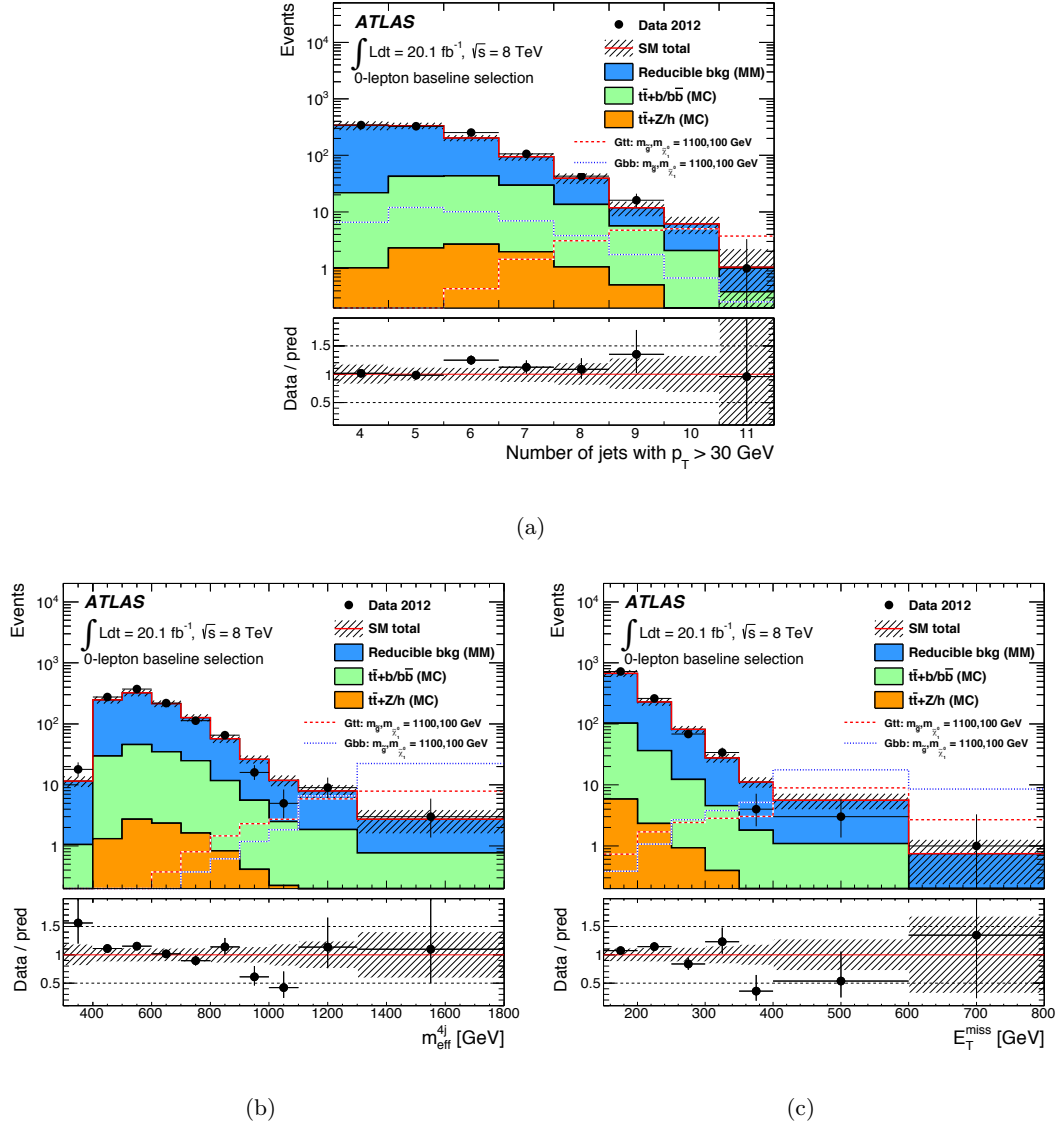
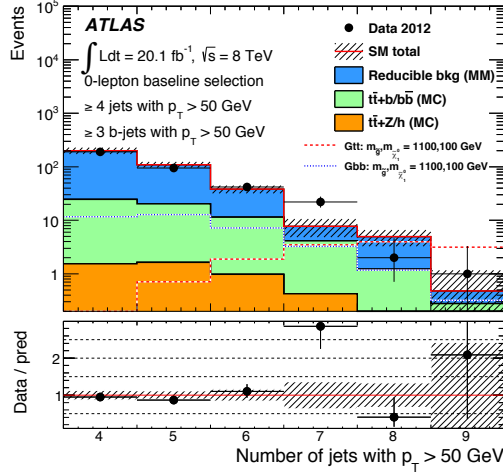
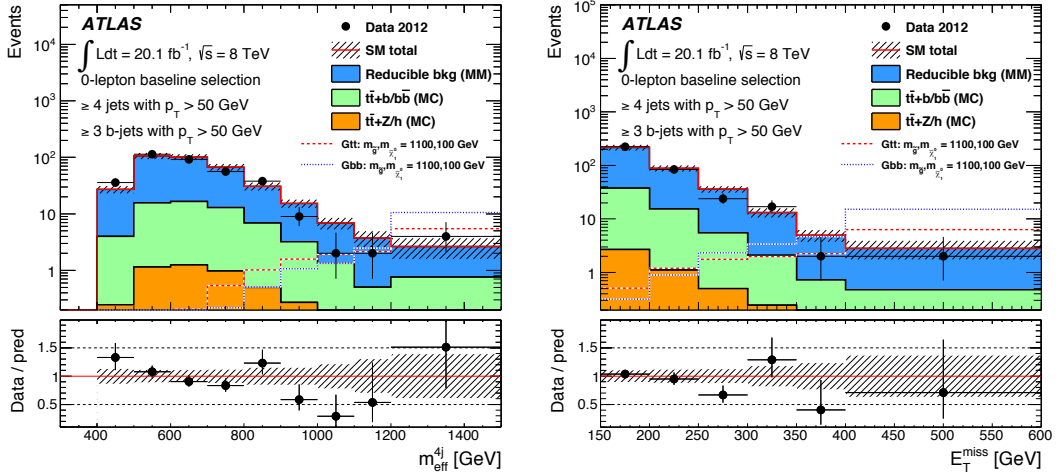


Figure 4. The observed distributions of (a) the number of jets with $p_T > 30$ GeV, (b) m_{eff}^{4j} and (c) E_T^{miss} after the 0-lepton baseline selection, together with the background prediction. Also displayed are the respective contributions of the backgrounds described in the legend and the ratio between the expected and observed event yields. The shaded bands include all experimental systematic uncertainties on the background prediction. The prediction for two signal points from the Gtt ($\tilde{g} \rightarrow t\bar{t}\chi_1^0$) and Gbb ($\tilde{g} \rightarrow b\bar{b}\chi_1^0$) models are overlaid. The normalisation of the irreducible background $t\bar{t} + b/b\bar{b}$ is as predicted by its theoretical cross-section scaled to the same luminosity as the data, prior to the fit in the control region.



(a)



(b)

(c)

Figure 5. The observed distributions of (a) the number of jets with $p_T > 50$ GeV, (b) m_{eff}^{4j} and (c) E_T^{miss} after requiring at least four jets with $p_T > 50$ GeV and at least three b -jets with $p_T > 50$ GeV in addition to the 0-lepton baseline selection, together with the background prediction. Also displayed are the respective contributions of the backgrounds described in the legend and the ratio between the expected and observed event yields. The shaded bands include all experimental systematic uncertainties on the background prediction. The prediction for two signal points from the Gtt ($\tilde{g} \rightarrow t\bar{t}\chi_1^0$) and Gbb ($\tilde{g} \rightarrow b\bar{b}\chi_1^0$) models are overlaid. The normalisation of the irreducible background $t\bar{t} + b/b\bar{b}$ is as predicted by its theoretical cross-section scaled to the same luminosity as the data, prior to the fit in the control region.

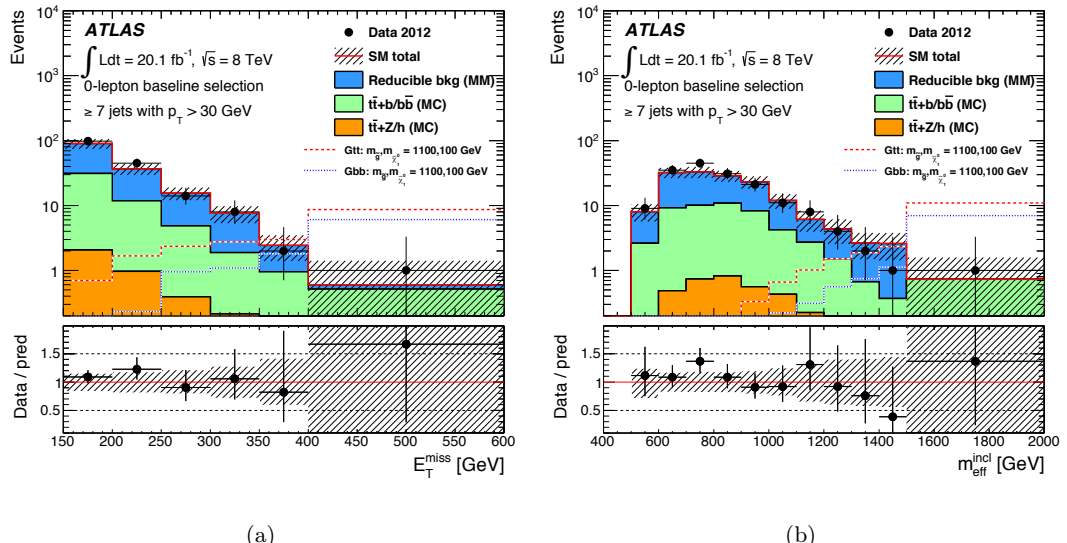


Figure 6. The (a) E_T^{miss} and (b) $m_{\text{eff}}^{\text{inel}}$ distributions observed in data after requiring at least seven jets with $p_T > 30$ GeV in addition to the 0-lepton baseline selection, together with the background prediction. Also displayed are the respective contributions of the backgrounds described in the legend and the ratio between the expected and observed event yields. The shaded bands include all experimental systematic uncertainties on the background prediction. The prediction for two signal points from the Gtt ($\tilde{g} \rightarrow t\bar{t}\tilde{\chi}_1^0$) and Gbb ($\tilde{g} \rightarrow b\bar{b}\tilde{\chi}_1^0$) models are overlaid. The normalisation of the irreducible background $t\bar{t} + b\bar{b}$ is as predicted by its theoretical cross-section scaled to the same luminosity as the data, prior to the fit in the control region.

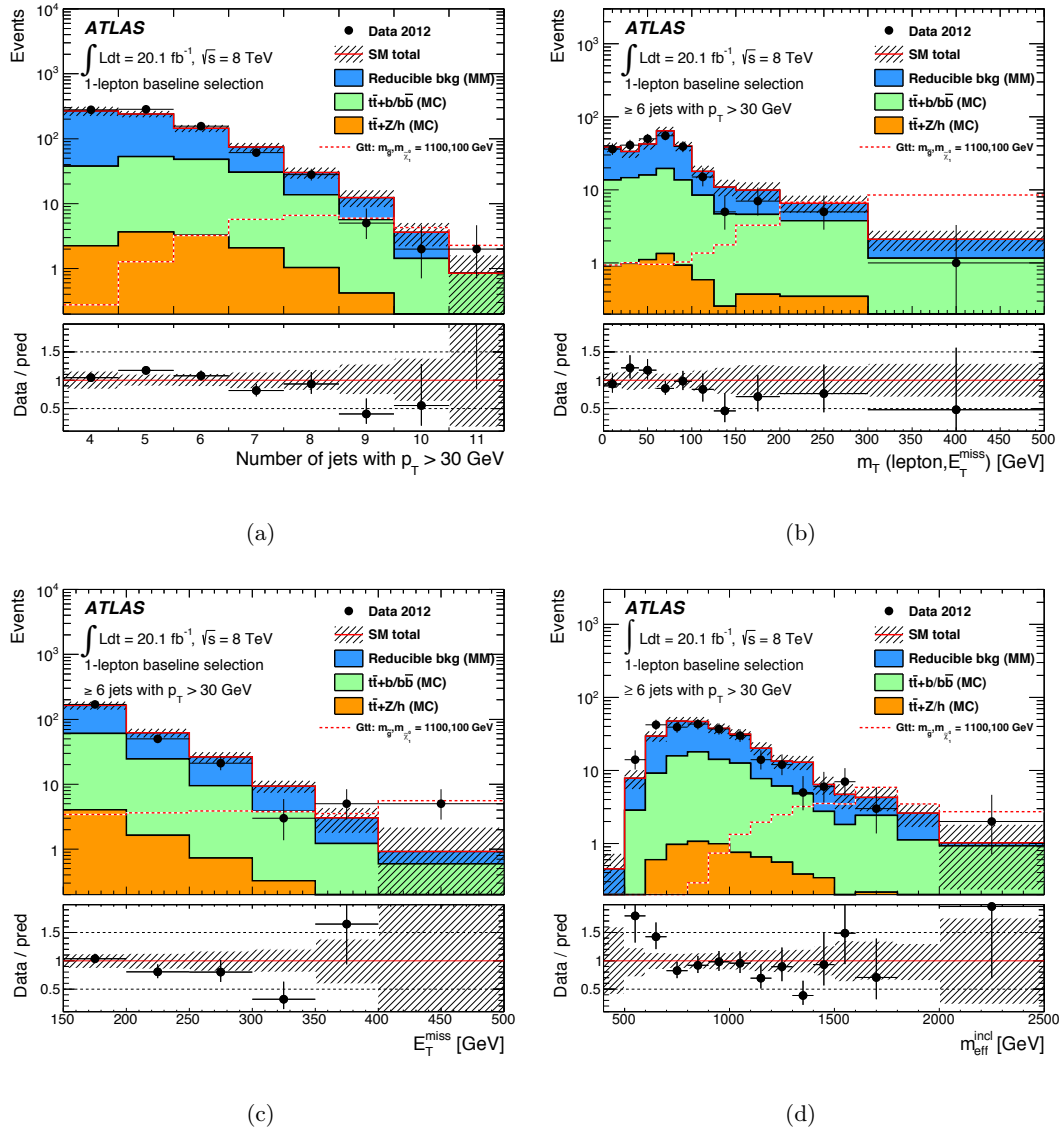


Figure 7. The distribution of (a) the number of jets with $p_T > 30$ GeV observed in data after the 1-lepton baseline selection, together with the background prediction. The (b) m_T , (c) E_T^{miss} and (d) $m_{\text{eff}}^{\text{incl}}$ distributions after requiring at least six jets $p_T > 30$ GeV in addition to the 1-lepton baseline selection are also shown. Also displayed are the respective contributions of the backgrounds described in the legend and the ratio between the expected and observed event yields. The shaded bands include all experimental systematic uncertainties on the background prediction. The prediction for one signal point from the Gtt ($\tilde{g} \rightarrow t\bar{t}\chi_1^0$) model is overlaid. The normalisation of the irreducible background $t\bar{t} + b/b\bar{b}$ is as predicted by its theoretical cross-section scaled to the same luminosity as the data, prior to the fit in the control region.

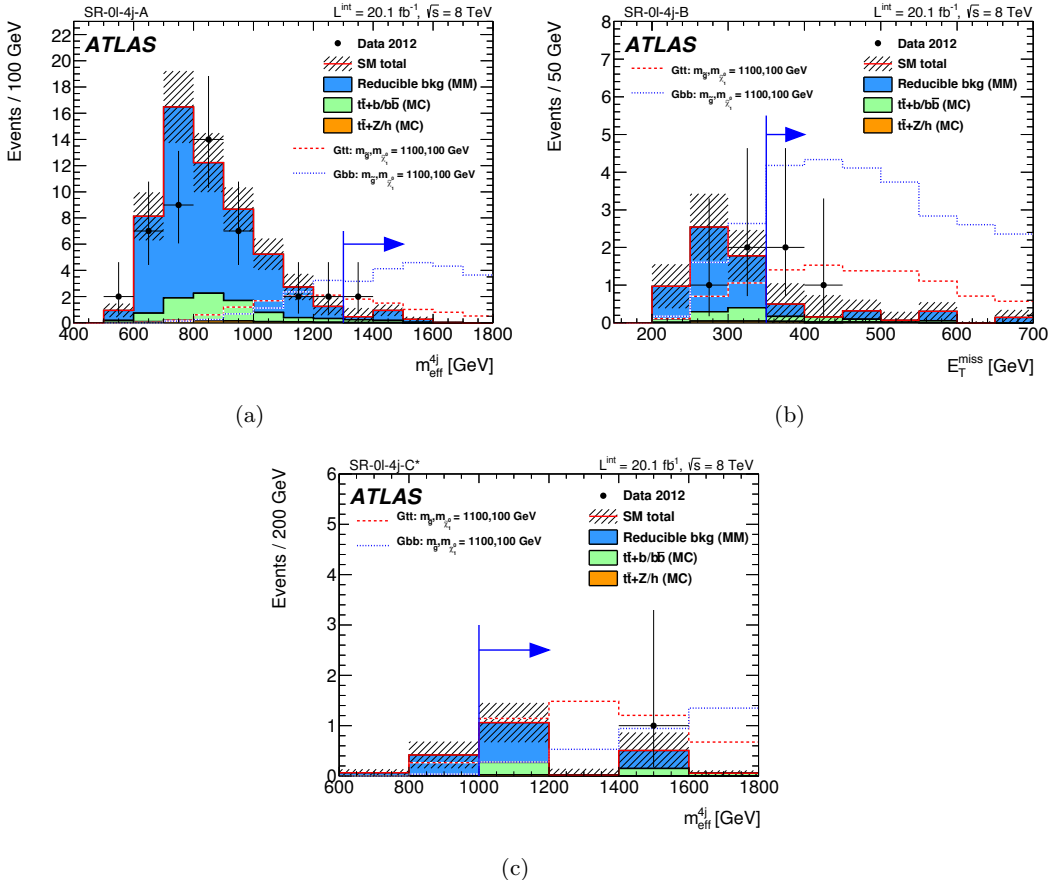


Figure 8. The (a)-(c) m_{eff}^{4j} and (b) E_T^{miss} distributions observed in data for SR-0 ℓ -4j-A, SR-0 ℓ -4j-B and SR-0 ℓ -4j-C*, respectively, after all requirements applied but the one indicated by the arrow, together with the background prediction. The shaded bands include all experimental systematic uncertainties on the background prediction. The prediction for two signal points from the Gtt ($\tilde{g} \rightarrow t\bar{t}\tilde{\chi}_1^0$) and Gbb ($\tilde{g} \rightarrow b\bar{b}\tilde{\chi}_1^0$) models are overlaid. The normalisation of the irreducible background $t\bar{t} + b/b\bar{b}$ is as predicted by its theoretical cross-section scaled to the same luminosity as the data, prior to the fit in the control region.

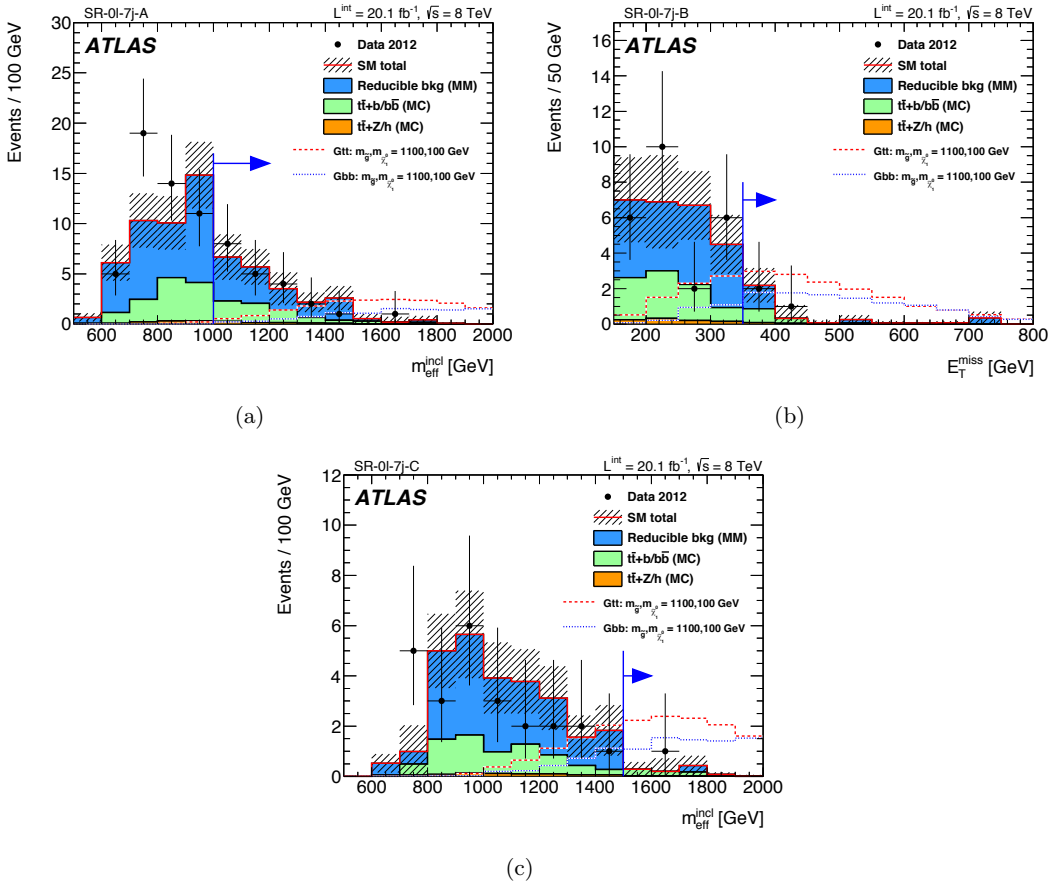


Figure 9. The (a)-(c) $m_{\text{eff}}^{\text{incl}}$ and (b) $E_{\text{T}}^{\text{miss}}$ distributions observed in data for SR-0 ℓ -7j-A, SR-0 ℓ -7j-B and SR-0 ℓ -7j-C, respectively, after all requirements applied but the one indicated by the arrow, together with the background prediction. The shaded bands include all experimental systematic uncertainties on the background prediction. The prediction for two signal points from the Gtt ($\tilde{g} \rightarrow t\bar{t}\tilde{\chi}_1^0$) and Gbb ($\tilde{g} \rightarrow b\bar{b}\tilde{\chi}_1^0$) models are overlaid. The normalisation of the irreducible background $t\bar{t} + b/b\bar{b}$ is as predicted by its theoretical cross-section scaled to the same luminosity as the data, prior to the fit in the control region.

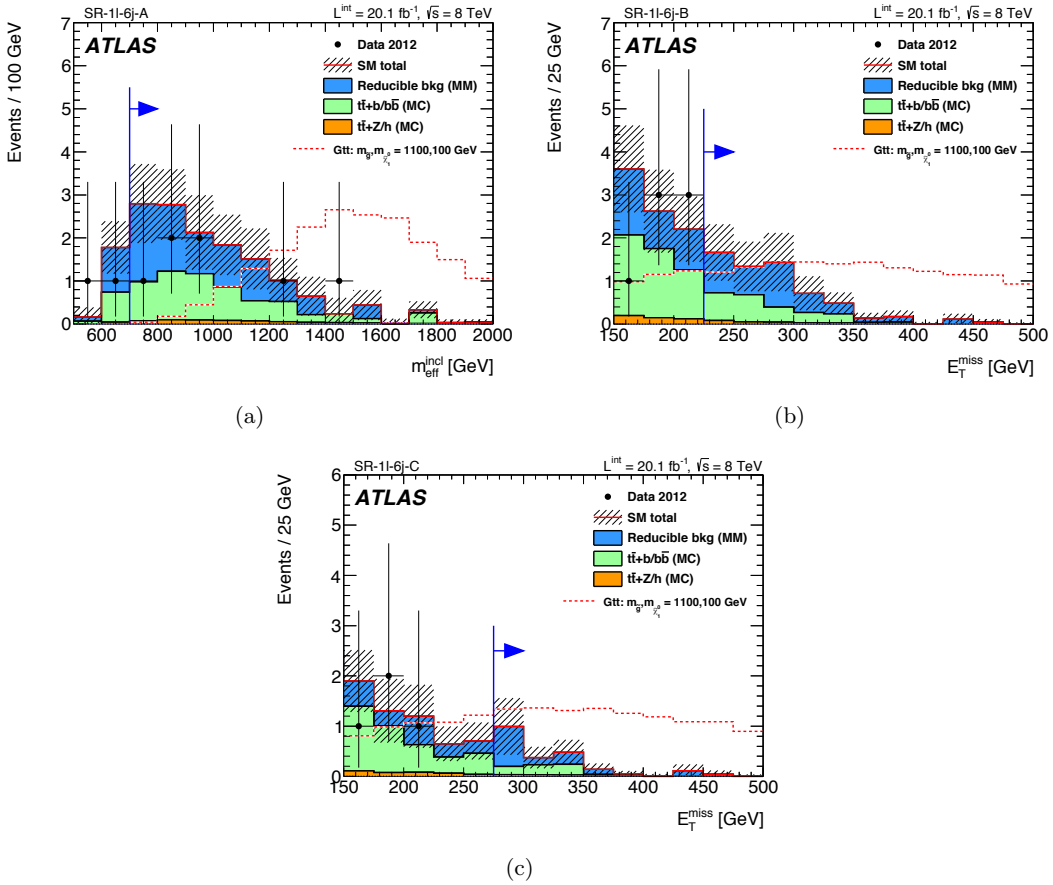


Figure 10. The (a) $m_{\text{eff}}^{\text{incl}}$ and (b)-(c) E_T^{miss} distribution observed in data for SR-1 ℓ -6j-A, SR-1 ℓ -6j-B and SR-1 ℓ -6j-C, respectively, after all requirements applied but the one indicated by the arrow, together with the background prediction. The shaded bands include all experimental systematic uncertainties on the background prediction. The prediction for one signal point from the Gtt ($\tilde{g} \rightarrow t\bar{t}\tilde{\chi}_1^0$) model is overlaid. The normalisation of the irreducible background $t\bar{t} + b/b\bar{b}$ is as predicted by its theoretical cross-section scaled to the same luminosity as the data, prior to the fit in the control region.

	SR-0 ℓ -4j-A	SR-0 ℓ -4j-B	SR-0 ℓ -4j-C*
Observed events	2	3	1
Fitted background events	1.6 ± 0.9	1.3 ± 0.9	1.6 ± 0.7
Reducible background events	1.1 ± 0.8	$0.7^{+0.8}_{-0.7}$	1.1 ± 0.5
$t\bar{t} + b/b\bar{b}$ events	0.4 ± 0.3	0.4 ± 0.3	0.4 ± 0.4
$t\bar{t} + (Z \rightarrow b\bar{b})$ events	0.03 ± 0.02	0.04 ± 0.03	0.01 ± 0.01
$t\bar{t} + (h \rightarrow b\bar{b})$ events	0.05 ± 0.05	0.07 ± 0.07	0.03 ± 0.03
MC-only prediction	2.6	3.7	2.3
CL_b	0.65	0.87	0.39
p_0	0.40	0.15	0.5
Expected UL on N_{BSM}	$4.5^{+1.7}_{-0.5} (4.3^{+2.6}_{-0.9})$	$4.5^{+1.7}_{-0.6} (4.3^{+2.6}_{-1.0})$	$4.1^{+1.7}_{-0.3} (4.1^{+2.2}_{-1.0})$
Observed UL on N_{BSM}	5.2 (5.0)	6.5 (6.2)	3.9 (3.8)
Observed (expected) UL on σ_{vis} [fb]	0.26 (0.22)	0.32 (0.22)	0.19 (0.20)
	SR-0 ℓ -7j-A	SR-0 ℓ -7j-B	SR-0 ℓ -7j-C
Observed events	21	3	1
Fitted background events	21.2 ± 4.6	3.2 ± 1.6	$0.9^{+1.0}_{-0.9}$
Reducible background events	13.6 ± 4.0	1.7 ± 1.2	< 0.65
$t\bar{t} + b/b\bar{b}$ events	6.7 ± 3.9	1.3 ± 1.1	0.8 ± 0.7
$t\bar{t} + (Z \rightarrow b\bar{b})$ events	0.3 ± 0.1	0.07 ± 0.03	0.03 ± 0.03
$t\bar{t} + (h \rightarrow b\bar{b})$ events	0.5 ± 0.5	0.1 ± 0.1	0.06 ± 0.06
MC-only prediction	31.4	6.8	3.1
CL_b	0.51	0.53	0.59
p_0	0.50	0.50	0.46
Expected UL on N_{BSM}	$13.8^{+4.7}_{-3.4} (13.5^{+5.3}_{-3.7})$	$6.0^{+2.2}_{-1.3} (5.9^{+2.5}_{-1.8})$	$4.1^{+1.6}_{-0.8} (4.1^{+2.1}_{-1.0})$
Observed UL on N_{BSM}	13.9 (13.4)	6.1 (5.8)	4.2 (4.1)
Observed (expected) UL on σ_{vis} [fb]	0.69 (0.69)	0.30 (0.30)	0.21 (0.20)

Table 4. Results of the likelihood fit in all 0-lepton signal regions. The errors shown include all systematic uncertainties. The data in the signal regions are not included in the fit. The MC-only predictions are given for comparison. The CL_b -values, which quantify the observed level of agreement with the expected yield, and the p_0 -values, which represent the probability of the SM background alone to fluctuate to the observed number of events or higher, are also reported. The p_0 -values are truncated at 0.5 if the number of observed events is below the number of expected events. Also shown are the expected and observed upper limits (UL) at 95% CL on the number of beyond-the-SM events N_{BSM} in each SR. These limits are derived with pseudo-experiments, and the results obtained with an asymptotic approximation are given in parentheses for comparison. They are used to derive upper limits on the visible cross-section $\sigma_{\text{vis}} = \sigma \times A \times \epsilon$ for hypothetical non-SM contributions.

	SR-1 ℓ -6j-A	SR-1 ℓ -6j-B	SR-1 ℓ -6j-C
Observed events	7	0	0
Fitted background events	13.5 ± 3.2	6.1 ± 1.8	2.3 ± 0.7
Reducible background events	7.2 ± 3.4	3.7 ± 1.9	1.5 ± 0.7
$t\bar{t} + b/b\bar{b}$ events	5.7 ± 3.1	2.1 ± 1.4	0.7 ± 0.5
$t\bar{t} + (Z \rightarrow b\bar{b})$ events	0.2 ± 0.1	0.11 ± 0.08	0.07 ± 0.03
$t\bar{t} + (h \rightarrow b\bar{b})$ events	0.4 ± 0.4	0.2 ± 0.2	0.08 ± 0.08
MC-only prediction	16.4	7.5	2.8
CL_b	0.10	0.02	0.17
p_0	0.50	0.50	0.50
Expected UL on N_{BSM}	$9.0^{+3.5}_{-2.3} (9.1^{+4.0}_{-2.8})$	$6.0^{+2.3}_{-1.7} (6.0^{+3.0}_{-1.9})$	$4.3^{+1.8}_{-0.5} (4.2^{+2.6}_{-0.9})$
Observed UL on N_{BSM}	6.1 (5.8)	3.5 (3.2)	3.6 (2.9)
Observed (expected) UL on σ_{vis} [fb]	0.30 (0.45)	0.17 (0.30)	0.18 (0.21)

Table 5. Results of the likelihood fit in all 1-lepton signal regions. The errors shown include all systematic uncertainties. The data in the signal regions are not included in the fit. The MC-only predictions are given for comparison. The CL_b -values, which quantify the observed level of agreement with the expected yield, and the p_0 -values, which represent the probability of the SM background alone to fluctuate to the observed number of events or higher, are also reported. The p_0 -values are truncated at 0.5 if the number of observed events is below the number of expected events. Also shown are the expected and observed upper limits (UL) at 95% CL on the number of beyond-the-SM events N_{BSM} in each SR. These limits are derived with pseudo-experiments and the results obtained with an asymptotic approximation are given in parentheses for comparison. They are used to derive upper limits on the visible cross-section $\sigma_{\text{vis}} = \sigma \times A \times \epsilon$ for hypothetical non-SM contributions.

10 Interpretations

The results are used to derive exclusion limits in the context of several SUSY models (see section 2) including bottom quarks or top quarks in the decay chain. The expected and observed exclusion limits are calculated using the asymptotic approximation for each SUSY model, treating the systematic uncertainties as fully correlated between the signal and the background and between the 0- and 1-lepton channels where appropriate, and including the expected signal contamination in the CR. Theoretical uncertainties on the SUSY signals are estimated as described in section 4. Limits are calculated for the nominal cross-section, and for the $\pm 1\sigma_{\text{theory}}^{\text{SUSY}}$ cross-sections. All limits quoted in the text correspond to the $-1\sigma_{\text{theory}}^{\text{SUSY}}$ hypothesis.

Limits are derived using the SR yielding the best expected sensitivity for each point in the parameter space, derived prior to having considered the data in the SR. For signal models where both the 0- and 1-lepton channels contribute to the sensitivity, these are combined in a simultaneous fit to enhance the sensitivity of the analysis. In this case, all possible permutations between the three 1-lepton and the six 0-lepton SRs are considered

for each point of the parameter space, and the best expected combination is used. The SR- 0ℓ -4j signal regions are mostly sensitive to the gluino decays $\tilde{g} \rightarrow b\bar{b}\tilde{\chi}_1^0$ via on-shell or off-shell sbottoms, whilst the SR- 0ℓ -7j and SR- 1ℓ -6j signal regions are used to set exclusion limits in models where top quark enriched final states are expected.

The expected and observed 95% CL exclusion limits obtained with the 0-lepton channel for the direct-sbottom model are presented in the $(m_{\tilde{b}_1}, m_{\tilde{\chi}_2^0})$ plane in figure 11. Sbottom masses between 340 GeV and 600 GeV are excluded for $m_{\tilde{\chi}_2^0} = 300$ GeV. No sensitivity is obtained for low $m_{\tilde{\chi}_2^0}$ due to the soft E_T^{miss} expected for these signal events. The sensitivity of this analysis to \tilde{b}_1 pair production processes where $\tilde{b}_1 \rightarrow b + \tilde{\chi}_2^0$, $\tilde{\chi}_2^0 \rightarrow h + \tilde{\chi}_1^0$, depends on $m_{\tilde{\chi}_1^0}$. For higher neutralino masses, the sensitivity decreases because of the tight E_T^{miss} and jet p_T selections applied in this analysis.

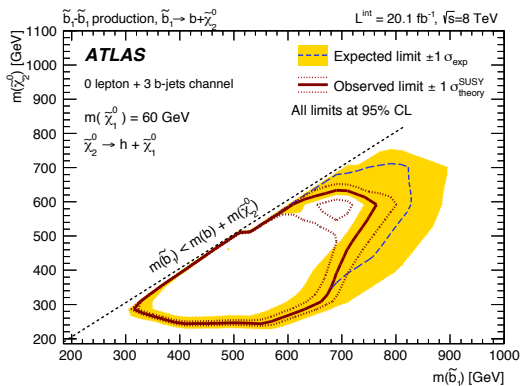


Figure 11. Exclusion limits in the $(m_{\tilde{b}_1}, m_{\tilde{\chi}_2^0})$ plane for the direct-sbottom model. The dashed blue and solid bold red lines show the 95% CL expected and observed limits respectively, including all uncertainties except the theoretical signal cross-section uncertainty. The shaded (yellow) bands around the expected limits show the impact of the experimental and background theoretical uncertainties while the dotted red lines show the impact on the observed limit of the variation of the nominal signal cross-section by 1σ of its theoretical uncertainty.

The expected and observed exclusion limits for the gluino-sbottom scenario are shown in figure 12 (a). Exclusion limits are presented in the $(m_{\tilde{g}}, m_{\tilde{b}_1})$ plane for the 0-lepton channel. Gluino masses below 1250 GeV are excluded for sbottom masses up to about 900 GeV. The result is complementary to the ATLAS search for direct sbottom pair production also carried out with 20.1 fb^{-1} of data at 8 TeV [92].

A combination of the 0- and 1-lepton results is used to derive the limit contours for the gluino-stop I and II models, presented in the $(m_{\tilde{g}}, m_{\tilde{t}_1})$ plane in figure 12 (b) and (c). Gluino masses below 1180 GeV are excluded for stop masses up to 1000 GeV in the gluino-stop I model, while gluino masses below 1190 GeV are excluded for stop masses up to 1000 GeV in the gluino-stop II model. The sensitivity is lower in the gluino-stop I model for most of the parameter space where soft E_T^{miss} and jets are expected from the chargino decay $\tilde{\chi}_1^\pm \rightarrow W^* \tilde{\chi}_1^0$. The result is complementary to the ATLAS searches for direct stop pair production performed in the 0-lepton channel with 20.1 fb^{-1} of data at 8 TeV [93] and in the 1-lepton channel with 4.7 fb^{-1} of data at 7 TeV [94].

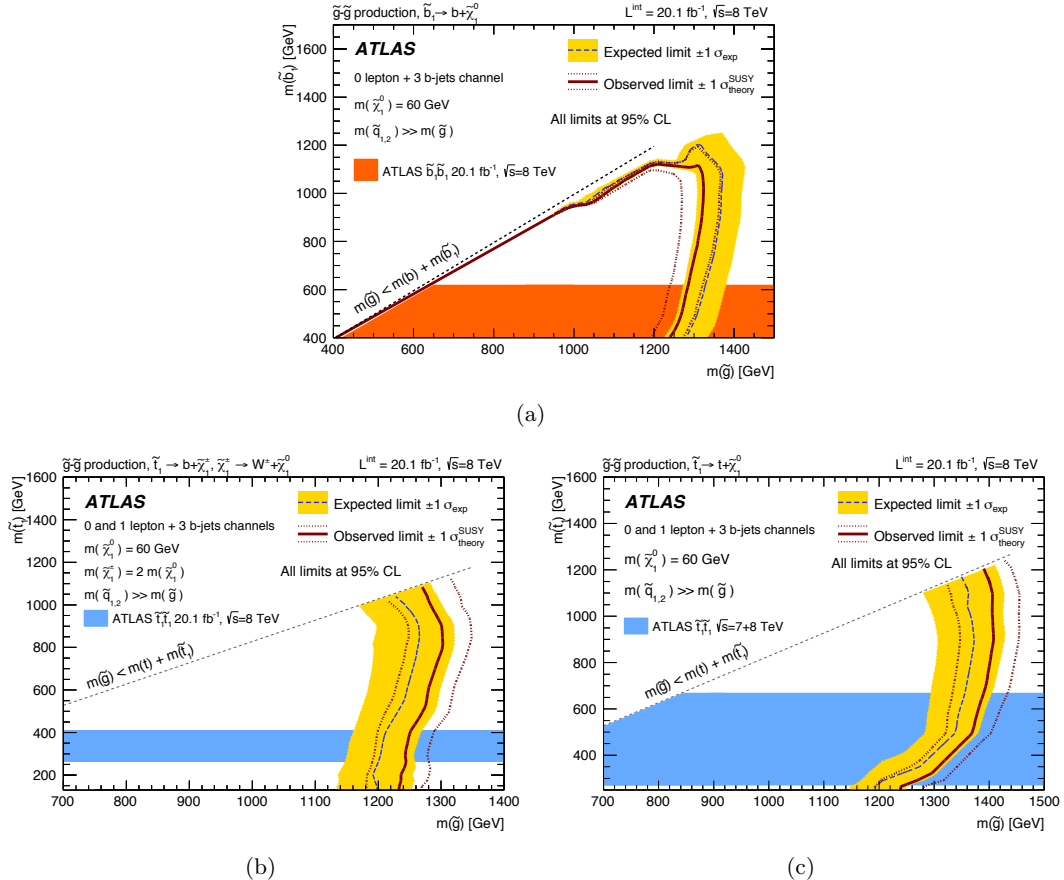


Figure 12. Exclusion limits in the $(m_{\tilde{g}}, m_{\tilde{b}_1})$ plane for the (a) gluino–sbottom model, and in the $(m_{\tilde{g}}, m_{\tilde{t}_1})$ plane for the gluino–stop (b) I and (c) II models. The dashed blue and solid bold red lines show the 95% CL expected and observed limits respectively, including all uncertainties except the theoretical signal cross-section uncertainty. The shaded (yellow) bands around the expected limits show the impact of the experimental and background theoretical uncertainties while the dotted red lines show the impact on the observed limit of the variation of the nominal signal cross-section by 1σ of its theoretical uncertainty. Also shown for reference are the results from the ATLAS sbottom and stop searches [92–94] derived using the nominal cross section.

The expected and observed exclusion limits for the Gbb model are shown in figure 13 (a). As for the gluino–sbottom model, four b -jets and E_T^{miss} are expected in the final state and only the 0-lepton channel is used for the interpretation. Gluino masses below 1250 GeV are excluded for $m_{\tilde{\chi}_1^0} < 400$ GeV while neutralino masses below 600 GeV are excluded for $m_{\tilde{g}} = 1000$ GeV. Lower sensitivity is achieved at very low mass splitting between the gluino and the neutralino because of the presence of soft b -jets and the low E_T^{miss} expected in signal events.

The combination of the 0-lepton and 1-lepton channels is used to obtain the exclusion contours for the Gtt model, displayed in figure 13 (b). Gluino masses below 1340 GeV are excluded for $m_{\tilde{\chi}_1^0} < 400$ GeV while neutralino masses below 620 GeV are excluded for

$m_{\tilde{g}} = 1000$ GeV. The SR-0 ℓ -7j signal regions have the best sensitivity at large mass splitting between the gluino and the neutralino, where hard jets and large E_T^{miss} are expected, while the 1-lepton SRs have a better sensitivity close to the kinematic boundary.

Figure 13 (c) shows the expected and observed exclusion limits for the Gtb scenario. The combination of the two channels is used to set the excluded area. Gluino masses below 1300 GeV are excluded for $m_{\tilde{\chi}_1^0} < 300$ GeV while neutralino masses below 600 GeV are excluded for $m_{\tilde{g}} = 1100$ GeV.

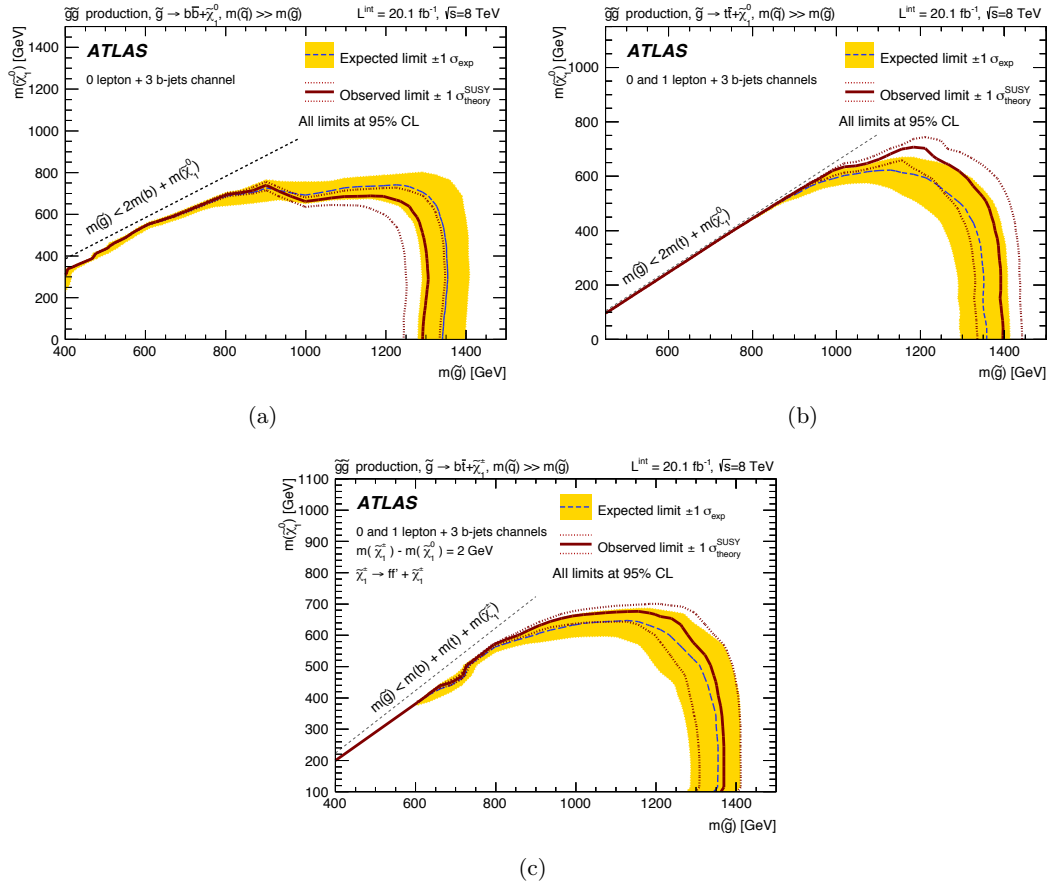


Figure 13. Exclusion limits in the $(m_{\tilde{g}}, m_{\tilde{\chi}_1^0})$ plane for the (a) Gbb, (b) Gtt and (c) Gtb models. The dashed blue and solid bold red lines show the 95% CL expected and observed limits respectively, including all uncertainties except the theoretical signal cross-section uncertainty. The shaded (yellow) bands around the expected limits show the impact of the experimental and background theoretical uncertainties while the dotted red lines show the impact on the observed limit of the variation of the nominal signal cross-section by 1σ of its theoretical uncertainty.

Finally, expected and observed 95% CL limits for the mSUGRA/CMSSM scenario discussed in section 2 are presented in the $(m_0, m_{1/2})$ plane in figure 14. Gluino masses smaller than 1280 GeV are excluded. This analysis is especially sensitive to the high m_0 region, where final states with four top quarks dominate.

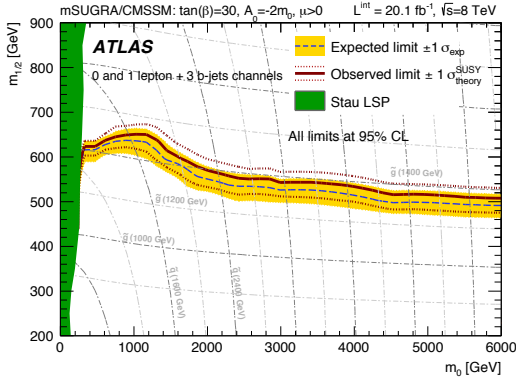


Figure 14. Exclusion limits in the $(m_0, m_{1/2})$ plane for the mSUGRA/CMSSM model. The dashed blue and solid bold red lines show the 95% CL expected and observed limits respectively, including all uncertainties except the theoretical signal cross-section uncertainty. The shaded (yellow) bands around the expected limits show the impact of the experimental and background theoretical uncertainties while the dotted red lines show the impact on the observed limit of the variation of the nominal signal cross-section by 1σ of its theoretical uncertainty.

11 Conclusions

A search is presented in this paper for pair production of gluinos and sbottoms decaying into final states with multi- b -jets and missing transverse momentum. This analysis uses 20.1 fb^{-1} of pp collisions at a centre-of-mass energy of 8 TeV collected by the ATLAS experiment at the LHC. Events with large missing transverse momentum, at least four to at least seven jets, and at least three b -jets are considered. The analysis is carried out separately for events with and without leptons in the final state, and the two channels are combined to enhance the sensitivity to SUSY scenarios with top quarks in the decay chain. No significant excess of events above SM expectations is found in data and the results are interpreted in the context of various simplified models involving gluinos, sbottoms and stops. In particular, gluino masses up to about 1340 GeV are excluded at 95% CL in some models.

Acknowledgments

We thank CERN for the very successful operation of the LHC, as well as the support staff from our institutions without whom ATLAS could not be operated efficiently.

We acknowledge the support of ANPCyT, Argentina; YerPhI, Armenia; ARC, Australia; BMWF and FWF, Austria; ANAS, Azerbaijan; SSTC, Belarus; CNPq and FAPESP, Brazil; NSERC, NRC and CFI, Canada; CERN; CONICYT, Chile; CAS, MOST and NSFC, China; COLCIENCIAS, Colombia; MSMT CR, MPO CR and VSC CR, Czech Republic; DNRF, DNSRC and Lundbeck Foundation, Denmark; EPLANET, ERC and NSRF, European Union; IN2P3-CNRS, CEA-DSM/IRFU, France; GNSF, Georgia; BMBF, DFG, HGF, MPG and AvH Foundation, Germany; GSRT and NSRF, Greece; ISF, MINERVA, GIF, I-CORE and Benoziyo Center, Israel; INFN, Italy; MEXT and JSPS, Japan;

CNRST, Morocco; FOM and NWO, Netherlands; BRF and RCN, Norway; MNiSW and NCN, Poland; GRICES and FCT, Portugal; MNE/IFA, Romania; MES of Russia and ROSATOM, Russian Federation; JINR; MSTD, Serbia; MSSR, Slovakia; ARRS and MIZS, Slovenia; DST/NRF, South Africa; MINECO, Spain; SRC and Wallenberg Foundation, Sweden; SER, SNSF and Cantons of Bern and Geneva, Switzerland; NSC, Taiwan; TAEK, Turkey; STFC, the Royal Society and Leverhulme Trust, United Kingdom; DOE and NSF, United States of America.

The crucial computing support from all WLCG partners is acknowledged gratefully, in particular from CERN and the ATLAS Tier-1 facilities at TRIUMF (Canada), NDGF (Denmark, Norway, Sweden), CC-IN2P3 (France), KIT/GridKA (Germany), INFN-CNAF (Italy), NL-T1 (Netherlands), PIC (Spain), ASGC (Taiwan), RAL (UK) and BNL (USA) and in the Tier-2 facilities worldwide.

References

- [1] H. Miyazawa, *Baryon Number Changing Currents*, *Prog. Theor. Phys.* **36** (6) (1966) 1266–1276.
- [2] P. Ramond, *Dual Theory for Free Fermions*, *Phys. Rev. D* **3** (1971) 2415–2418.
- [3] Y. A. Gol’fand and E. P. Likhtman, *Extension of the Algebra of Poincare Group Generators and Violation of p Invariance*, *JETP Lett.* **13** (1971) 323–326.
- [4] A. Neveu and J. H. Schwarz, *Factorizable dual model of pions*, *Nucl. Phys. B* **31** (1971) 86–112.
- [5] A. Neveu and J. H. Schwarz, *Quark Model of Dual Pions*, *Phys. Rev. D* **4** (1971) 1109–1111.
- [6] J. Gervais and B. Sakita, *Field theory interpretation of supergauges in dual models*, *Nucl. Phys. B* **34** (1971) 632–639.
- [7] D. V. Volkov and V. P. Akulov, *Is the Neutrino a Goldstone Particle?*, *Phys. Lett. B* **46** (1973) 109–110.
- [8] J. Wess and B. Zumino, *A Lagrangian Model Invariant Under Supergauge Transformations*, *Phys. Lett. B* **49** (1974) 52.
- [9] J. Wess and B. Zumino, *Supergauge Transformations in Four-Dimensions*, *Nucl. Phys. B* **70** (1974) 39–50.
- [10] S. Dimopoulos and H. Georgi, *Softly Broken Supersymmetry and SU(5)*, *Nucl. Phys. B* **193** (1981) 150.
- [11] E. Witten, *Dynamical Breaking of Supersymmetry*, *Nucl. Phys. B* **188** (1981) 513.
- [12] M. Dine, W. Fischler, and M. Srednicki, *Supersymmetric Technicolor*, *Nucl. Phys. B* **189** (1981) 575–593.
- [13] S. Dimopoulos and S. Raby, *Supercolor*, *Nucl. Phys. B* **192** (1981) 353.
- [14] N. Sakai, *Naturalness in Supersymmetric Guts*, *Zeit. Phys. C* **11** (1981) 153.
- [15] R. Kaul and P. Majumdar, *Cancellation of quadratically divergent mass corrections in globally supersymmetric spontaneously broken gauge theories*, *Nucl. Phys. B* **199** (1982) 36.

- [16] P. Fayet, *Supersymmetry and Weak, Electromagnetic and Strong Interactions*, *Phys. Lett.* **B 64** (1976) 159.
- [17] P. Fayet, *Spontaneously Broken Supersymmetric Theories of Weak, Electromagnetic and Strong Interactions*, *Phys. Lett.* **B 69** (1977) 489.
- [18] G. R. Farrar and P. Fayet, *Phenomenology of the Production, Decay, and Detection of New Hadronic States Associated with Supersymmetry*, *Phys. Lett.* **B 76** (1978) 575–579.
- [19] P. Fayet, *Relations Between the Masses of the Superpartners of Leptons and Quarks, the Goldstino Couplings and the Neutral Currents*, *Phys. Lett.* **B 84** (1979) 416.
- [20] R. Barbieri and G. Giudice, *Upper Bounds on Supersymmetric Particle Masses*, *Nucl. Phys.* **B 306** (1988) 63.
- [21] B. de Carlos and J. Casas, *One loop analysis of the electroweak breaking in supersymmetric models and the fine tuning problem*, *Phys. Lett.* **B 309** (1993) 320–328, [[hep-ph/9303291](#)].
- [22] ATLAS Collaboration, *Search for top and bottom squarks from gluino pair production in final states with missing transverse energy and at least three b-jets with the ATLAS detector*, *Eur. Phys. J.* **C 72** (2012) 2174, [[arXiv:1207.4686](#)].
- [23] ATLAS Collaboration, *Search for new phenomena in final states with large jet multiplicities and missing transverse momentum at $\sqrt{s} = 8$ TeV proton-proton collisions using the ATLAS experiment*, *JHEP* **10** (2013) 130, [[arXiv:1308.1841](#)].
- [24] ATLAS Collaboration, *Search for supersymmetry at $\sqrt{s}=8$ TeV in final states with jets and two same-sign leptons or three leptons with the ATLAS detector*, *JHEP* **1406** (2014) 035, [[arXiv:1404.2500](#)].
- [25] CMS Collaboration, *Search for gluino mediated bottom- and top-squark production in multijet final states in pp collisions at 8 TeV*, *Phys. Lett.* **B 725** (2013) 243–270, [[arXiv:1305.2390](#)].
- [26] CMS Collaboration, *Search for supersymmetry in pp collisions at $\sqrt{s} = 8$ TeV in events with a single lepton, large jet multiplicity, and multiple b jets*, *Phys. Lett.* **B 733** (2014) 328–353, [[arXiv:1311.4937](#)].
- [27] CMS Collaboration, *Search for new physics in events with same-sign dileptons and jets in pp collisions at $\sqrt{s} = 8$ TeV*, *JHEP* **01** (2014) 163, [[arXiv:1311.6736](#)].
- [28] CMS Collaboration, *Search for new physics in the multijet and missing transverse momentum final state in proton-proton collisions at $\sqrt{s} = 8$ TeV*, *JHEP* **06** (2014) 055, [[arXiv:1402.4770](#)].
- [29] A. H. Chamseddine, R. Arnowitt, and P. Nath, *Locally supersymmetric grand unification*, *Phys. Rev. Lett.* **49** (1982) 970.
- [30] R. Barbieri, S. Ferrara, and C. A. Savoy, *Gauge Models with Spontaneously Broken Local Supersymmetry*, *Phys. Lett.* **B 119** (1982) 343.
- [31] L. E. Ibanez, *Locally Supersymmetric SU(5) Grand Unification*, *Phys. Lett.* **B 118** (1982) 73.
- [32] L. J. Hall, J. D. Lykken, and S. Weinberg, *Supergravity as the Messenger of Supersymmetry Breaking*, *Phys. Rev.* **D 27** (1983) 2359–2378.
- [33] N. Ohta, *Grand Unified Theories Based on Local Supersymmetry*, *Prog. Theor. Phys.* **70** (1983) 542.

- [34] G. L. Kane, C. F. Kolda, L. Roszkowski, and J. D. Wells, *Study of constrained minimal supersymmetry*, *Phys. Rev.* **D 49** (1994) 6173–6210.
- [35] ATLAS Collaboration, *The ATLAS Experiment at the CERN Large Hadron Collider*, *JINST* **3** (2008) S08003.
- [36] ATLAS Collaboration, *Improved luminosity determination in pp collisions at $\sqrt{s} = 7$ TeV using the ATLAS detector at the LHC*, *Eur. Phys. J.* **C 73** (2013) 2518, [[arXiv:1302.4393](#)].
- [37] P. Nason, *A New method for combining NLO QCD with shower Monte Carlo algorithms*, *JHEP* **11** (2004) 040, [[hep-ph/0409146](#)].
- [38] S. Frixione, P. Nason, and C. Oleari, *Matching NLO QCD computations with Parton Shower simulations: the POWHEG method*, *JHEP* **11** (2007) 070, [[arXiv:0709.2092](#)].
- [39] S. Alioli, P. Nason, C. Oleari, and E. Re, *A general framework for implementing NLO calculations in shower Monte Carlo programs: the POWHEG BOX*, *JHEP* **06** (2010) 043, [[arXiv:1002.2581](#)].
- [40] M. Cacciari, M. Czakon, M. Mangano, A. Mitov, and P. Nason, *Top-pair production at hadron colliders with next-to-next-to-leading logarithmic soft-gluon resummation*, *Phys. Lett.* **B 710** (2012) 612–622, [[arXiv:1111.5869](#)].
- [41] P. Barnreuther, M. Czakon, and A. Mitov, *Percent Level Precision Physics at the Tevatron: First Genuine NNLO QCD Corrections to $q\bar{q} \rightarrow t\bar{t} + X$* , *Phys. Rev. Lett.* **109** (2012) 132001, [[arXiv:1204.5201](#)].
- [42] M. Czakon and A. Mitov, *NNLO corrections to top-pair production at hadron colliders: the all-fermionic scattering channels*, *JHEP* **12** (2012) 054, [[arXiv:1207.0236](#)].
- [43] M. Czakon and A. Mitov, *NNLO corrections to top pair production at hadron colliders: the quark-gluon reaction*, *JHEP* **01** (2013) 080, [[arXiv:1210.6832](#)].
- [44] M. Czakon, P. Fiedler, and A. Mitov, *The total top quark pair production cross-section at hadron colliders through $\mathcal{O}(\alpha_S^4)$* , *Phys. Rev. Lett.* **110** (2013) 252004, [[arXiv:1303.6254](#)].
- [45] M. Czakon and A. Mitov, *Top++: A Program for the Calculation of the Top-Pair Cross-Section at Hadron Colliders*, [arXiv:1112.5675](#).
- [46] P. Z. Skands, *Tuning Monte Carlo Generators: The Perugia Tunes*, *Phys. Rev.* **D 82** (2010) 074018, [[arXiv:1005.3457](#)].
- [47] H.-L. Lai, M. Guzzi, J. Huston, Z. Li, P. M. Nadolsky, et al., *New parton distributions for collider physics*, *Phys. Rev.* **D 82** (2010) 074024, [[arXiv:1007.2241](#)].
- [48] T. Sjöstrand, S. Mrenna, and P. Z. Skands, *PYTHIA 6.4 Physics and Manual*, *JHEP* **05** (2006) 026, [[hep-ph/0603175](#)].
- [49] ATLAS Collaboration, *ATLAS tunes of PYTHIA 6 and PYTHIA 8 for MC11*, *ATL-PHYS-PUB-2011-009* (2011).
- [50] G. Corcella, I. Knowles, G. Marchesini, S. Moretti, K. Odagiri, et al., *HERWIG 6: An Event generator for hadron emission reactions with interfering gluons (including supersymmetric processes)*, *JHEP* **01** (2001) 010, [[hep-ph/0011363](#)].
- [51] J. Alwall, M. Herquet, F. Maltoni, O. Mattelaer, and T. Stelzer, *MadGraph 5 : Going Beyond*, *JHEP* **06** (2011) 128.

- [52] B. P. Kersevan and E. Richter-Was, *The Monte Carlo event generator AcerMC versions 2.0 to 3.8 with interfaces to PYTHIA 6.4, HERWIG 6.5 and ARIADNE 4.1*, *Comput. Phys. Commun.* **184** (2013) 919–985, [[hep-ph/0405247](#)].
- [53] N. Kidonakis, *Next-to-next-to-leading-order collinear and soft gluon corrections for t-channel single top quark production*, *Phys. Rev. D* **83** (2011) 091503, [[arXiv:1103.2792](#)].
- [54] J. Pumplin, D. Stump, J. Huston, H. Lai, P. M. Nadolsky, et al., *New generation of parton distributions with uncertainties from global QCD analysis*, *JHEP* **07** (2002) 012, [[hep-ph/0201195](#)].
- [55] S. Frixione and B. R. Webber, *Matching NLO QCD computations and parton shower simulations*, *JHEP* **0206** (2002) 029, [[hep-ph/0204244](#)].
- [56] S. Frixione, E. Laenen, P. Motylinski, and B. R. Webber, *Single-top production in MC@NLO*, *JHEP* **0603** (2006) 092, [[hep-ph/0512250](#)].
- [57] N. Kidonakis, *NNLL resummation for s-channel single top quark production*, *Phys. Rev. D* **81** (2010) 054028, [[arXiv:1001.5034](#)].
- [58] N. Kidonakis, *Two-loop soft anomalous dimensions for single top quark associated production with a W^- or H^-* , *Phys. Rev. D* **82** (2010) 054018, [[arXiv:1005.4451](#)].
- [59] M. Garzelli, A. Kardos, C. Papadopoulos, and Z. Trocsanyi, *$t\bar{t}W^{+-}$ and $t\bar{t}Z$ Hadroproduction at NLO accuracy in QCD with Parton Shower and Hadronization effects*, *JHEP* **11** (2012) 056, [[arXiv:1208.2665](#)].
- [60] S. Dittmaier, C. Mariotti, G. Passarino, R. Tanaka, A. Alekhin, et al., *Handbook of LHC Higgs Cross Sections: 2. Differential Distributions*, [arXiv:1201.3084](#).
- [61] ATLAS Collaboration, *Summary of ATLAS PYTHIA 8 tunes*, ATL-PHYS-PUB-2012-003 (2012).
- [62] T. Sjostrand, S. Mrenna, and P. Z. Skands, *A Brief Introduction to PYTHIA 8.1*, *Comput. Phys. Commun.* **178** (2008) 852–867, [[arXiv:0710.3820](#)].
- [63] S. Catani, L. Cieri, G. Ferrera, D. de Florian, and M. Grazzini, *Vector boson production at hadron colliders: A Fully exclusive QCD calculation at NNLO*, *Phys. Rev. Lett.* **103** (2009) 082001, [[arXiv:0903.2120](#)].
- [64] A. Martin, W. Stirling, R. Thorne, and G. Watt, *Parton distributions for the LHC*, *Eur. Phys. J. C* **63** (2009) 189–285, [[arXiv:0901.0002](#)].
- [65] T. Binoth, M. Ciccolini, N. Kauer, and M. Kramer, *Gluon-induced W -boson pair production at the LHC*, *JHEP* **12** (2006) 046, [[hep-ph/0611170](#)].
- [66] M. Bähr et al., *Herwig++ Physics and Manual*, *Eur. Phys. J. C* **58** (2008) 639–707, [[arXiv:0803.0883](#)].
- [67] W. Beenakker, R. Hopker, M. Spira, and P. Zerwas, *Squark and gluino production at hadron colliders*, *Nucl. Phys. B* **492** (1997) 51–103, [[hep-ph/9610490](#)].
- [68] A. Kulesza and L. Motyka, *Threshold resummation for squark-antisquark and gluino-pair production at the LHC*, *Phys. Rev. Lett.* **102** (2009) 111802, [[arXiv:0807.2405](#)].
- [69] A. Kulesza and L. Motyka, *Soft gluon resummation for the production of gluino-gluino and squark-antisquark pairs at the LHC*, *Phys. Rev. D* **80** (2009) 095004, [[arXiv:0905.4749](#)].

- [70] W. Beenakker, S. Brensing, M. Kramer, A. Kulesza, E. Laenen, et al., *Soft-gluon resummation for squark and gluino hadroproduction*, *JHEP* **12** (2009) 041, [[arXiv:0909.4418](https://arxiv.org/abs/0909.4418)].
- [71] W. Beenakker, S. Brensing, M. Kramer, A. Kulesza, E. Laenen, et al., *Squark and Gluino Hadroproduction*, *Int. J. Mod. Phys. A* **26** (2011) 2637–2664, [[arXiv:1105.1110](https://arxiv.org/abs/1105.1110)].
- [72] M. Krämer, A. Kulesza, R. van der Leeuw, M. Mangano, S. Padhi, et al., *Supersymmetry production cross sections in pp collisions at $\sqrt{s} = 7 \text{ TeV}$* , [arXiv:1206.2892](https://arxiv.org/abs/1206.2892).
- [73] ATLAS Collaboration, *The ATLAS Simulation Infrastructure*, *Eur. Phys. J. C* **70** (2010) 823–874, [[arXiv:1005.4568](https://arxiv.org/abs/1005.4568)].
- [74] S. Agostinelli, J. Allison, K. Amako, J. Apostolakis, H. Araujo, et al., *Geant4 simulation toolkit*, *Nucl. Instrum. Meth. A* **506** (2003) 250–303.
- [75] ATLAS Collaboration, The simulation principle and performance of the ATLAS fast calorimeter simulation fastcalosim, ATL-PHYS-PUB-2010-013, <https://cds.cern.ch/record/1300517> (2010).
- [76] M. Cacciari, G. Salam, and G. Soyez, *The anti- k_t jet clustering algorithm*, *JHEP* **04** (2008) 063, [[arXiv:0802.1189](https://arxiv.org/abs/0802.1189)].
- [77] ATLAS Collaboration, *Jet energy measurement with the ATLAS detector in proton-proton collisions at $\sqrt{s} = 7 \text{ TeV}$* , *Eur. Phys. J. C* **73** (2013) 2304, [[arXiv:1112.6426](https://arxiv.org/abs/1112.6426)].
- [78] M. Cacciari and G. P. Salam, *Pileup subtraction using jet areas*, *Phys. Lett. B* **659** (2008) 119–126, [[arXiv:0707.1378](https://arxiv.org/abs/0707.1378)].
- [79] ATLAS Collaboration, *Measurement of the b-tag Efficiency in a Sample of Jets Containing Muons with 5 fb^{-1} of Data from the ATLAS Detector*, *ATLAS-CONF-2012-043* (2012).
- [80] ATLAS Collaboration, *b-jet tagging calibration on c-jets containing D^* mesons*, *ATLAS-CONF-2012-039* (2012).
- [81] ATLAS Collaboration, *Measurement of the Mistag Rate of b-tagging algorithms with 5 fb^{-1} of Data Collected by the ATLAS Detector*, *ATLAS-CONF-2012-040* (2012).
- [82] ATLAS Collaboration, *Calibration of b-tagging using dileptonic top pair events in a combinatorial likelihood approach with the ATLAS experiment*, *ATLAS-CONF-2014-004* (2012).
- [83] ATLAS Collaboration, *Electron reconstruction and identification efficiency measurements with the ATLAS detector using the 2011 LHC proton-proton collision data*, [arXiv:1404.2240](https://arxiv.org/abs/1404.2240).
- [84] ATLAS Collaboration, *Preliminary results on the muon reconstruction efficiency, momentum resolution, and momentum scale in ATLAS 2012 pp collision data*, *ATLAS-CONF-2013-088* (2013).
- [85] ATLAS Collaboration, *Performance of missing transverse momentum reconstruction in proton-proton collisions at 7 TeV with ATLAS*, *Eur. Phys. J. C* **72** (2012) 1844, [[arXiv:1108.5602](https://arxiv.org/abs/1108.5602)].
- [86] ATLAS Collaboration, *Characterisation and mitigation of beam-induced backgrounds observed in the ATLAS detector during the 2011 proton-proton run*, *JINST* **8** (2013) P07004, [[arXiv:1303.0223](https://arxiv.org/abs/1303.0223)].

- [87] **ATLAS** Collaboration, *Measurement of the top quark-pair production cross section with ATLAS in pp collisions at $\sqrt{s} = 7$ TeV*, *Eur. Phys. J. C* **71** (2011) 1577, [[arXiv:1012.1792](#)].
- [88] G. Cowan, K. Cranmer, E. Gross, and O. Vitells, *Asymptotic formulae for likelihood-based tests of new physics*, *Eur. Phys. J. C* **71** (2011) 1554.
- [89] **ATLAS** Collaboration, *Single hadron response measurement and calorimeter jet energy scale uncertainty with the ATLAS detector at the LHC*, *Eur. Phys. J. C* **73** (2013) 2305, [[arXiv:1203.1302](#)].
- [90] J. Pumplin, D. Stump, R. Brock, D. Casey, J. Huston, et al., *Uncertainties of predictions from parton distribution functions. 2. The Hessian method*, *Phys. Rev. D* **65** (2001) 014013, [[hep-ph/0101032](#)].
- [91] A. L. Read, *Presentation of search results: the CL_s technique*, *Journal of Physics G: Nuclear and Particle Physics* **28** (2002), no. 10 2693.
- [92] **ATLAS** Collaboration, *Search for direct third-generation squark pair production in final states with missing transverse momentum and two b-jets in $\sqrt{s} = 8$ TeV pp collisions with the ATLAS detector*, *JHEP* **10** (2013) 189, [[arXiv:1308.2631](#)].
- [93] **ATLAS** Collaboration, *Search for direct pair production of the top squark in all-hadronic final states in proton-proton collisions at $\sqrt{s} = 8$ TeV with the ATLAS detector*, [`arXiv:1406.1122`](#).
- [94] **ATLAS** Collaboration, *Search for direct top squark pair production in final states with one isolated lepton, jets, and missing transverse momentum in $\sqrt{s} = 7$ TeV pp collisions using 4.7 fb^{-1} of ATLAS data*, *Phys. Rev. Lett.* **109** (2012) 211803, [[arXiv:1208.2590](#)].

Process: Gtt model			
Point: $m_g = 1200 \text{ GeV}$, $m_{\tilde{\chi}_1^0} = 100 \text{ GeV}$			
Selection	Total events passed	Scaled to 20.1 fb^{-1}	Efficiency
Initial	99999	88.4	100%
preselection			
Event quality cuts	97025	85.7	97.0%
≥ 4 jets with $p_T > 30 \text{ GeV}$	96713	85.4	96.7%
≥ 1 jet with $p_T > 90 \text{ GeV}$	96588	85.3	96.6%
$E_T^{\text{miss}} > 150 \text{ GeV}$	86489	76.4	86.5%
≥ 3 b-jets with $p_T > 30 \text{ GeV}$	39573	32.6	36.9%
0-lepton preselection			
lepton veto	19636	16.3	18.4%
$\Delta\phi_{\text{min}}^{4j} > 0.5$	14082	11.7	13.2%
$E_T^{\text{miss}}/m_{\text{eff}}^{4j} > 0.2$	12281	10.2	11.5%
≥ 7 jets with $p_T > 30 \text{ GeV}$	11998	10.0	11.3%
SR-0l-7j-A			
$E_T^{\text{miss}} > 200 \text{ GeV}$	11743	9.7	11.0%
$m_{\text{eff}}^{\text{incl}} > 1000 \text{ GeV}$	11641	9.7	10.9%
SR-0l-7j-B			
$E_T^{\text{miss}} > 350 \text{ GeV}$	8863	7.4	8.3%
$m_{\text{eff}}^{\text{incl}} > 1000 \text{ GeV}$	8855	7.4	8.3%
SR-0l-7j-C			
$E_T^{\text{miss}} > 250 \text{ GeV}$	11085	9.2	10.4%
$m_{\text{eff}}^{\text{incl}} > 1500 \text{ GeV}$	8923	7.3	8.3%
1-lepton preselection			
≥ 1 -lepton with $p_T > 25 \text{ GeV}$	16878	13.8	15.6%
≥ 6 jets with $p_T > 30 \text{ GeV}$	14324	11.8	13.3%
SR-1l-6j-A			
$E_T^{\text{miss}} > 175 \text{ GeV}$	13699	11.3	12.8%
$m_T > 140 \text{ GeV}$	10640	8.8	9.9%
$m_{\text{eff}}^{\text{incl}} > 700 \text{ GeV}$	10640	8.8	9.9%
SR-1l-6j-B			
$E_T^{\text{miss}} > 225 \text{ GeV}$	12205	10.0	11.4%
$m_T > 140 \text{ GeV}$	9622	7.9	9.0%
$m_{\text{eff}}^{\text{incl}} > 800 \text{ GeV}$	9621	7.9	9.0%
SR-1l-6j-C			
$E_T^{\text{miss}} > 275 \text{ GeV}$	10576	8.7	9.8%
$m_T > 160 \text{ GeV}$	8129	6.7	7.6%
$m_{\text{eff}}^{\text{incl}} > 900 \text{ GeV}$	8127	6.7	7.6%